iLTM: Integrated Large Tabular Model

David Bonet^{1,2,*} Marçal Comajoan Cara^{1,3,*}

Alvaro Calafell⁴

Daniel Mas Montserrat¹

Alexander G. Ioannidis^{1,2}

¹Stanford University ²University of California, Santa Cruz ³University of California, Berkeley ⁴École Polytechnique

Abstract

Tabular data underpins decisions across science, industry, and public services. Despite rapid progress, advances in deep learning have not fully carried over to the tabular domain, where gradient-boosted decision trees (GBDTs) remain a default choice in practice. We present iLTM, an integrated Large Tabular Model that unifies tree-derived embeddings, dimensionality-agnostic representations, a metatrained hypernetwork, multilayer perceptrons (MLPs), and retrieval within a single architecture. Pretrained on more than 1,800 heterogeneous classification datasets, iLTM achieves consistently superior performance across tabular classification and regression tasks, from small datasets to large and high-dimensional tasks. After light fine-tuning, the meta-trained hypernetwork transfers to regression targets, matching or surpassing strong baselines. Extensive experiments show that iLTM outperforms well-tuned GBDTs and leading deep tabular models while requiring less task-specific tuning. By bridging the gap between tree-based and neural methods, iLTM offers a new framework for tabular foundation models for robust, adaptable, and scalable tabular learning.

1 Introduction

Tabular data is one of the most common data structures in real-world applications, including health-care, logistics, finance, and countless administrative tasks. Despite its ubiquity, recent advances in large-scale foundation models that have transformed natural language processing, vision, and other domains [1, 2, 3], have not yet transferred equivalently to tabular data [4]. Although significant progress has been made in developing neural network architectures for tabular data [5, 6], and in adapting existing foundation models [7, 8], no single approach consistently excels across the full spectrum of tabular tasks. These tasks range from small datasets with mixed feature types to extremely large and high-dimensional tables. As a result, gradient-boosted decision trees (GBDTs) have remained the dominant choice for real-world tabular applications and automation tasks, largely due to their robust performance and ease of use. However, GBDTs and other classical models must be trained and hyperparameter-tuned independently for each new task, an approach that becomes prohibitively time-consuming in large-scale or highly diverse settings. This limitation underscores the need for a *foundation model* in the tabular domain—one that is pre-trained on thousands of examples, with learned knowledge of the tabular domain, and capable of delivering strong performance across heterogeneous tasks without exhaustive retraining.

Addressing this performance gap has motivated a recent call for Large Tabular Models (LTMs) [9] to bring the success of foundation models in other domains to tabular learning. Simple neural architectures based on multilayer perceptrons (MLPs) have been shown to be a good fit for tabular

^{*} Equal contribution. Correspondence: ioannidis@stanford.edu

data, achieving performance comparable to GBDTs when paired with proper preprocessing [10] and parameter tuning [11]. However, comprehensive evaluations like TabZilla [12] reveal a critical insight: no single technique consistently excels across the diverse landscape of tabular tasks.

This observation reflects the inherent heterogeneity of tabular data, from small datasets with mixed feature types to large-scale, high-dimensional tables. Different architectural paradigms have emerged to address specific aspects of this challenge. While neural networks offer flexibility and representational power [5, 6], they may not always capture the specific inductive biases inherent in tabular data, where GBDTs tend to excel [13, 14, 12]. Recent work on in-context learning for tabular data has demonstrated remarkable effectiveness in learning new tasks without retraining [15, 16, 17, 18]. Moreover, research on tabular meta-learning has shown how hypernetworks can be applied to pretrain on vast amounts of datasets that are not necessarily the ones used during inference [16, 17], paralleling how large-scale pre-training has revolutionized deep learning models in domains such as text [1], vision [3], and speech [19]. Furthermore, another promising direction has been in retrieval-augmented classification approaches, which have shown competitive performance in many tabular datasets [20, 21], though with limitations in others [22].

Recognizing that no single technique consistently outperforms others across the diverse landscape of tabular datasets, we propose an integrated approach. In this work, we introduce iLTM (Figure 1), an integrated Large Tabular Model that combines the strengths of gradient boosted decision trees, metalearned hypernetworks, retrieval-augmented classification, and strong MLP architectures within a single model. Our experiments reveal that the same weights, meta-trained exclusively on classification, can be fine-tuned to regression targets, highlighting promising adaptation and cross-task transfer capability for tabular foundation models. iLTM is the first integrated architecture combining GBDT embeddings, hypernetwork, retrieval and MLP with large-scale pre-training on real tabular data, showing predictive power superior to other neural methods and a stronger capacity to adapt to datasets of different sizes and configurations.

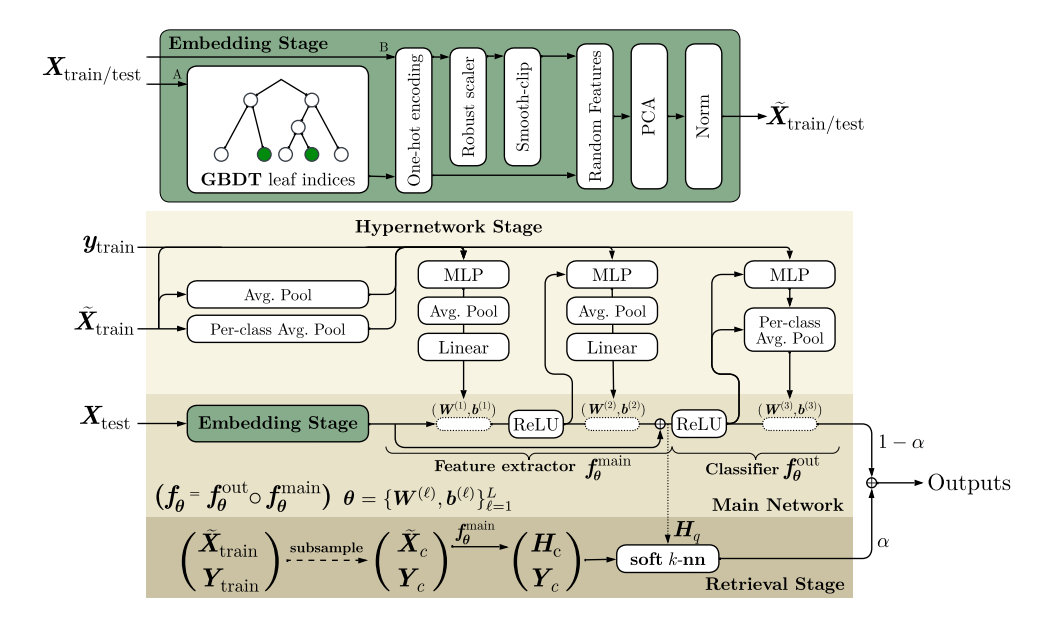


Figure 1: Overview of the iLTM architecture. Raw tabular datasets pass through GBDT embeddings and/or robust preprocessing, then a dimensionality-agnostic representation feeds a meta-trained hypernetwork that generates the MLP layers (3 layers, 512 hidden units) of the main network. The main network predictions are augmented with retrieval weighted by α .

Contributions. Overall, our main contributions are:

- (i) A novel neural-tree hybrid: We present iLTM, a method that integrates GBDTs, hypernetworks, retrieval modules, and strong MLPs into a single architecture specifically tailored for tabular data.
- (ii) **Large-scale meta-training**: We pre-train the hypernetwork on thousands of real-world tabular classification tasks, covering a broad range of data structures, which later enables cross-task transfer to regression datasets.
- (iii) **Strong performance across tasks**: iLTM generally outperforms the best hyperparameter-tuned GBDT and deep tabular models on classification and regression benchmarks.
- (iv) A new path for robust adaptability: Our model design maintains competitive performance from small, low-dimensional tasks to large, high-dimensional complex datasets while requiring less task-specific overhead.
- (v) We provide an open-source implementation and release our model weights to facilitate future research and applications of LTMs: https://github.com/AI-sandbox/iLTM.

2 Related Work

Pre-training and Meta-training Pre-training has become a cornerstone in machine learning, where large models are trained on extensive data collections, and later adapted to downstream tasks [1, 3]. In the context of tabular data, however, the shift towards pre-trained or meta-learned models is only recent. A prominent line of work started with TabPFN [15, 18], pre-training a Transformer model on synthetic small tabular data. HyperFast [16] demonstrated scalability to larger datasets, meta-learning a hypernetwork on real tabular datasets, and XTab [23] also found pre-training on more tasks leading to increased performance. CARTE [24] proposed a pre-training scheme on a knowledge based on graph representations, and TabLLM [8] fine-tuned LLMs with serialized tables, but it struggles handling numerical features in a setting originally formulated for natural language. Other work has explored pre-training diffusion models for tabular data generation [25], and meta-learning for few-shot learning in semi-supervised settings [26].

Neural Network-only Tabular Models Multilayer perceptrons (MLPs) remain a fundamental neural approach for tabular data [6]. With proper preprocessing and hyperparameter optimization, MLPs can approach or match GBDTs on certain benchmarks [11, 10]. Attention-based models proposed [27, 28, 29, 15, 30] incorporate specialized mechanisms for feature interactions, but struggle to scale efficiently for large or high-dimensional tables. In contrast, simpler yet effective MLP-based methods scale to larger datasets and retain competitive accuracy across diverse tasks while being more robust to hyperparameter variations.

Retrieval-Augmented Tabular Models Retrieval-augmented models have shown remarkable success across domains, from LLMs [31] to vision [32]. These approaches enhance model predictions by first retrieving relevant examples from training data and then incorporating them into the prediction process, effectively combining the benefits of local pattern recognition [33] with learned representations. For tabular data, retrieval mechanisms offer another pathway for enhancing model performance, particularly in the presence of sparse features or rare categories. Recent methods like TabR [20] and ModernNCA [21] incorporate nearest-neighbor information to refine learned representations. However, retrieval-based methods can be sensitive to the quality and scalability of the underlying retrieval index, potentially limiting their applicability when tables grow large or contain diverse feature types [22].

Tree Models and Neural-Tree Hybrids Ensembles of decision trees [34], such as random forests [35] and GBDTs [36, 37, 38], have long dominated tabular benchmarks due to their strong inductive biases and resilience to heterogeneous and missing features [5]. They often outperform purely neural architectures when extensively tuned [13, 14]. Several methods merge tree-based inductive biases with deep networks [27, 39, 40, 41, 42, 43], sometimes improving interpretability or feature selection, but they generally lag behind well-optimized GBDTs on large-scale tasks [13, 12]. While leveraging GBDTs as feature extractors has been shown to improve performance of probabilistic linear and neural classifiers [44, 40], a unified Large Tabular Model that effectively integrates tree-based and neural approaches has yet to be achieved.

3 iLTM: Integrated Large Tabular Model

Notation We consider tabular datasets \mathcal{D} with N data points and d features $\{(\boldsymbol{x}_i,y_i)\}_{i=1}^N \in \mathbb{R}^d \times \mathcal{Y}$, and we focus on binary and multi-class classification where $\mathcal{Y} := \{1,\ldots,K\}$ and K is the number of classes in the target. In matrix form, $\boldsymbol{X} \in \mathbb{R}^{N \times d}$ contains data points as rows, and the label vector $\boldsymbol{y} \in \mathcal{Y}^N$, the corresponding class labels. We assume that the dataset \mathcal{D} can be partitioned into training, testing, and optionally validation subsets, denoted as $\mathcal{D}_{\text{train}}$, $\mathcal{D}_{\text{test}}$, and \mathcal{D}_{val} , respectively.

3.1 Embedding Stage

In iLTM, the raw tabular features take two possible paths that act as preprocessing and initial transformations: a) obtaining a GBDT-based embedding, described in Section 3.1.1, and b) a preprocessing pipeline formalized in [10], that one-hot encodes categorical columns, imputes missing values as zero, and robustly scales and smooth-clips all resulting columns. This combination produces well-conditioned features, which has shown to improve performance in simple MLPs without excessive sensitivity to scale or outliers. After the initial transformations, the data representations undergo a randomized fixed-size embedding projection, described in Section 3.1.2.

3.1.1 GBDT Embedding

We construct a GBDT-based embedding by fitting a GBDT parametrized by γ on a labeled set. Formally, let $\{\text{tree}_t\}_{t=1}^T$ be the ensemble of T decision trees, each partitioning the input space into disjoint leaf regions. However, a tree t may only split along a subset of d_t dimensions. We denote by L_t the number of leaves in treet. A point $\boldsymbol{x}_i \in \mathbb{R}^d$ falls into exactly one leaf for each tree, producing a leaf index $l_i(\boldsymbol{x}) \in \{1,\dots,L_t\}$. We then define the GBDT embedding function $\Gamma_\gamma \colon \mathbb{R}^d \to \{0,1\}^M$ with $M = \sum_{t=1}^T L_t$ by concatenating the one-hot encodings of $l_t(\boldsymbol{x})$ across all $t \in \{1,\dots,T\}$. Figure 2 illustrates the induced partitioning of the input space for a single tree into leaf regions, how data points are assigned to leaves, and how the final one-hot encoding is constructed across an ensemble, producing a high-dimensional sparse binary representation of the input data, obtaining $\Gamma_\gamma(\boldsymbol{X}) \in \{0,1\}^{N \times M}$.

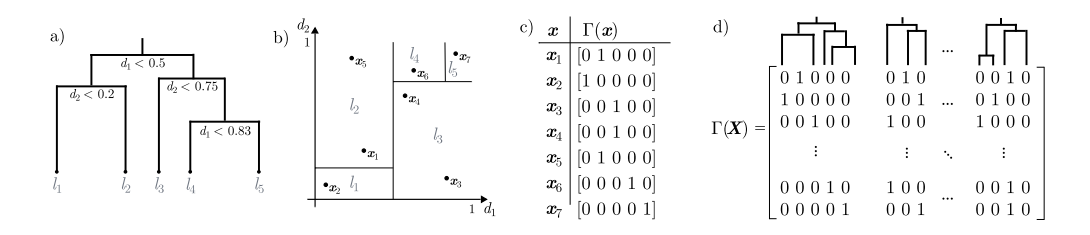


Figure 2: GBDT embedding process. (a) Decision tree splits on d_1 and d_2 leading to leaves $\{l_1, \ldots, l_5\}$. (b) 2D visualization of datapoints assigned to leaf cells. (c) Each data point is transformed into a one-hot vector. (d) Concatenated one-hot encodings across trees in the ensemble obtaining a sparse binary matrix $\Gamma(X)$.

This embedding incorporates the inductive biases of decision trees, and is robust to uninformative features. Additionally, some modern GBDT frameworks (such as CatBoost [37] and XGBoost [36]) handle categorical variables and missing values natively, improving robustness to incomplete or mixed-type datasets. By construction, $\Gamma(x)$ is non-smooth in x (stepwise transitions at tree-split boundaries). While MLPs alone typically learn smoother functions [13], combining them with GBDT embeddings can capture irregular patterns more effectively. We empirically observed that using embeddings of non-boosted tree ensembles such as with Random Forests [35, 45], generally led to a smaller increase in performance compared to GBDT-based ones. Finally, we also consider concatenating $\Gamma(x)$ with the features obtained after the preprocessing pipeline described in Section 3.1 to form a unified numerical-categorical representation input to the subsequent layers. We intentionally keep this GBDT component vanilla and under-tuned, because its role is not to match the performance of a well-tuned GBDT, but to generate informative sparse embeddings, while the performance gains come from feeding these embeddings with the MLP generated by the meta-trained hypernetwork and the retrieval component.

3.1.2 Fixed-size Embedding Projection

We define the complete *Embedding Stage* as a function $\Psi_{\gamma,\omega}: \mathbb{R}^d \to \mathbb{R}^{d_{\text{main}}}$, that processes the raw features into a fixed-size embedding $\tilde{x} \in \mathbb{R}^{d_{\text{main}}}$. Let $\psi(x) \in \mathbb{R}^m$ denote the output of the initial transformations (either preprocessing-only, GBDT embedding, or their concatenation). Hence, $\psi(x)$ may have dimension $m \neq d$. We then construct \tilde{x} via three steps: random feature expansion, PCA-based dimensionality reduction, and feature-wise normalization. First, we project $\psi(x)$ into \mathbb{R}^r via random features [46]:

where $\sigma(\cdot)$ is a pointwise nonlinearity (e.g. ReLU) and $\Omega \in \mathbb{R}^{m \times r}$. Random features can approximate certain kernels, and in this case we approximate the arc-cosine kernel, as it creates sparse, neural network-like representations [47], capturing rich nonlinear behavior. We choose r large enough to preserve information but still enable subsequent efficient dimension reduction. Then, we reduce from r to d_{main} by applying principal component analysis (PCA) to the randomized features,

$$\sigma(\mathbf{\Omega}^ op \psi(x)) \; \mapsto \; oldsymbol{U}^ op ig(\sigma(\mathbf{\Omega}^ op \psi(x)) - oldsymbol{\mu}ig) \; \in \; \mathbb{R}^{d_{ ext{main}}}.$$

where μ is the mean of the expanded features for the training batch and $U \in \mathbb{R}^{r \times d_{\text{main}}}$ contains the top d_{main} principal components, thus approximating Kernel PCA [48]. We follow the procedure in [16], but we further normalize each \tilde{x}_{ij} by

$$\tilde{x}_{ij} \leftarrow \frac{\tilde{x}_{ij} - \mu_j}{\sqrt{\sigma_j^2 + \epsilon}}.$$

where μ_j and σ_j are the mean and standard deviation of column j in a training batch \tilde{X} . Thus, $\Psi_{\gamma,\omega}(x_i) = \tilde{x}_i \in \mathbb{R}^{d_{\text{main}}}$ produces a manageable dimensionality-agnostic embedding for the main network, independent of input size or data type.

3.2 Main Network

For a dataset \mathcal{D} , a meta-model g_{ϕ} generates the parameters $\boldsymbol{\theta}$ of a specialized main network $f_{\boldsymbol{\theta}}$. This main network processes inputs $\tilde{\boldsymbol{x}} \in \mathbb{R}^{d_{\text{main}}}$ to obtain output logits:

$$f_{\boldsymbol{\theta}}(\tilde{\boldsymbol{x}}): \mathbb{R}^{d_{\text{main}}} \to \mathbb{R}^{K}$$
 (1)

The hypernetwork generates weights θ based on the training set representations X_{train} and the associated labels y_{train} , allowing the main network to adapt to the specific characteristics of each task.

3.2.1 Retrieval-Augmented Prediction

The main network incorporates a parameter-free retrieval mechanism inspired by ModernNCA [21], which operates as a soft k-nearest neighbors in the learned representation space [49, 50]. Let $f_{\boldsymbol{\theta}} = f_{\boldsymbol{\theta}}^{\text{out}} \circ f_{\boldsymbol{\theta}}^{\text{main}}$ denote our main network, where $f_{\boldsymbol{\theta}}^{\text{main}} : \mathbb{R}^{d_{\text{main}}} \to \mathbb{R}^{d_{\text{main}}}$ outputs the penultimate layer representations and $f_{\boldsymbol{\theta}}^{\text{out}} : \mathbb{R}^{d_{\text{main}}} \to \mathbb{R}^K$ is the final classification layer. Given a query batch $Q \in \mathbb{R}^{B \times d}$ and a context set $\{X_c, Y_c\}$ where $Y_c \in \{0, 1\}^{N_c \times K}$, the retrieval proceeds as follows:

1. Extract penultimate layer representations:

$$\boldsymbol{H}_q = f_{\boldsymbol{\theta}}^{\mathrm{main}}(\Psi_{\boldsymbol{\gamma}, \boldsymbol{\omega}}(\boldsymbol{Q})) \in \mathbb{R}^{B \times d_{\mathrm{main}}}, \quad \boldsymbol{H}_c = f_{\boldsymbol{\theta}}^{\mathrm{main}}(\Psi_{\boldsymbol{\gamma}, \boldsymbol{\omega}}(\boldsymbol{X}_c)) \in \mathbb{R}^{N_c \times d_{\mathrm{main}}}$$
 (2)

2. Compute cosine similarities between query and context representations:

$$\boldsymbol{S} = \boldsymbol{H}_{q} \boldsymbol{H}_{c}^{\top} / (\|\boldsymbol{H}_{q}\|_{2} \|\boldsymbol{H}_{c}\|_{2}) \in \mathbb{R}^{B \times N_{c}}$$
(3)

3. Apply temperature scaling and compute class logits via weighted label aggregation:

$$O_{\text{retrieval}} = SY_c/\tau \in \mathbb{R}^{B \times K}$$
 (4)

where $\tau > 0$ adjusts the similarity distribution sharpness.

The final prediction logits combine the main network and retrieval outputs:

$$O = (1 - \alpha) f_{\theta}^{\text{out}}(H_q) + \alpha O_{\text{retrieval}}$$
(5)

where $\alpha \in [0,1]$ controls the retrieval contribution. When $\alpha = 0$, we have $\mathbf{O} = f_{\boldsymbol{\theta}}^{\text{out}}(\mathbf{H}_q) = f_{\boldsymbol{\theta}}(\mathbf{Q})$, reducing to standard prediction using only the main network. The retrieval mechanism can be activated during inference regardless of the training configuration; however, hypernetworks trained with retrieval should generate networks with embeddings better suited for similarity-based predictions.

3.3 Hypernetwork Stage

We define the meta-model g_{ϕ} as a hypernetwork [51] that generates the parameters $\boldsymbol{\theta} = \{\boldsymbol{W}^{(\ell)}, \boldsymbol{b}^{(\ell)}\}_{\ell=1}^L$ of the main network $f_{\boldsymbol{\theta}}$ for each dataset \mathcal{D} . Unlike standard approaches that train a separate model for each dataset, g_{ϕ} is trained on a collection $\mathcal{M}_{\text{train}}$ of datasets and learns to produce $\boldsymbol{\theta}$ for any new dataset at test time.

The hypernetwork g_{ϕ} generates the L layers sequentially, as illustrated in Figure 1. Given an embedded generation set $\tilde{X}_{\text{gen}} \in \mathbb{R}^{N_{\text{gen}} \times d_{\text{main}}}$ and labels $Y_{\text{gen}} \in \{0,1\}^{N_{\text{gen}} \times K}$, we obtain the global and per-class means, concatenate it with the generation set, and feed it to MLP blocks $g_{\phi,\text{MLP}}^{(\ell)}$, consistent with the methodology proposed in [16]. For $\ell > 1$, it additionally conditions on the previously generated layer outputs. We then perform on the obtained representations an average pooling over the sample dimension, producing a single dataset-level embedding $z^{(\ell)} \in \mathbb{R}^h$. For $\ell < L$, the hypernetwork projects $z^{(\ell)}$ through a final linear layer:

$$[\boldsymbol{W}^{(\ell)}, \boldsymbol{b}^{(\ell)}] = g_{oldsymbol{\phi}, \mathrm{lin}}^{(\ell)}(\boldsymbol{z}^{(\ell)}).$$

A residual connection of $\hat{\boldsymbol{X}}_{\text{gen}}$ is added into the output of the penultimate layer L-1, preserving information from the *Embedding Stage* Ψ and stabilizing hypernetwork training. For the last layer L, let $\boldsymbol{z}_k^{(L)} \in \mathbb{R}^{d_{\text{main}}+1}$ be the average-pooled embedding for class k after $g_{\phi}^{(L)}$. We generate $\boldsymbol{W}_k^{(L)}$ and $\boldsymbol{b}_k^{(L)}$ from $\boldsymbol{z}_k^{(L)}$ and form $\boldsymbol{W}^{(L)}$ by stacking $\{\boldsymbol{W}_1^{(L)},\dots,\boldsymbol{W}_K^{(L)}\}$ row-wise, with a similar stacking for biases $\boldsymbol{b}^{(L)}$. During meta-training, we optimize ϕ over a collection of datasets $\mathcal{M}_{\text{train}}$ to minimize:

$$\min_{oldsymbol{\phi}} \mathbb{E}_{\mathcal{D} \sim \mathcal{M}_{ ext{train}}} \Big[\mathcal{L} \Big(f_{g_{oldsymbol{\phi}}(\mathcal{D}_{ ext{train}})} ig(\Psi(\mathcal{D}_{ ext{test}}) ig), oldsymbol{y}_{ ext{test}} \Big) \Big].$$

At test time, we fix ϕ^* and generate θ for unseen tasks.

3.4 Training iLTM

Algorithm 1 shows the meta-training process for iLTM. In practice, to avoid repeated overhead, we fit the GBDT-based embeddings and/or the robust preprocessing pipeline *off-line*, storing the embedding parameters γ . We use both XGBoost [36] and CatBoost [37] libraries for GBDT implementation. We consider three main variants of the embedding stage: (i) GBDT-only, (ii) robust preprocessing-only, or (iii) a concatenation of both. These approaches are interchangeable within the same meta-training procedure and each provides different inductive biases. In the algorithm below, we show a simplified version where γ (from GBDT or preprocessing) is already available.

For classification with K classes and labels $y_i \in \{0,1\}^K$, we use the standard cross-entropy loss:

$$\mathcal{L}_{\text{CE}}(f_{\boldsymbol{\theta}}(\tilde{\boldsymbol{x}}_i), \boldsymbol{y}_i) = -\sum_{k=1}^{K} (y_i)_k \log(\operatorname{softmax}(f_{\boldsymbol{\theta}}(\tilde{\boldsymbol{x}}_i))_k).$$

The total loss is averaged over the *gradient set* $X_{\text{grad}} \subset \mathcal{D}_{\text{train}}$, providing gradients to update ϕ .

Algorithm 1 iLTM Meta-training

```
Input: Meta-collection \mathcal{M}_{\text{train}}, hypernetwork g_{\phi}, learning rate \eta, accumulation size A.
Initialize \phi
for iteration = 1 to MaxSteps do
       \nabla_{\phi} \leftarrow 0 {Reset accumulated gradient}
      for a=1 to A do
            Sample a dataset \mathcal{D} \in \mathcal{M}_{train}
            Load or compute embedding parameters \gamma (off-line)
            Choose a generation subset (\boldsymbol{X}_{\text{gen}}, \boldsymbol{y}_{\text{gen}}) \subset \mathcal{D}_{\text{train}}
             \tilde{\boldsymbol{X}}_{\text{gen}},\, \boldsymbol{\omega} \leftarrow \Psi_{\boldsymbol{\gamma}}(\boldsymbol{X}_{\text{gen}})
            m{	heta} \leftarrow g_{m{\phi}}(	ilde{m{X}}_{	ext{gen}}, \, m{Y}_{	ext{gen}}) {Generate main weights} Choose a gradient subset (m{X}_{	ext{grad}}, m{y}_{	ext{grad}}) \subset \mathcal{D}_{	ext{train}}
            \hat{\boldsymbol{y}}_{\mathrm{grad}} \leftarrow f_{\boldsymbol{\theta}} (\Psi_{\boldsymbol{\gamma}, \boldsymbol{\omega}}(\boldsymbol{X}_{\mathrm{grad}}))
             \begin{array}{l} \mathcal{L} \leftarrow \mathcal{L}_{\text{CE}}(\hat{\pmb{y}}_{\text{grad}}, \pmb{y}_{\text{grad}}) \text{ {(Cross-entropy loss)}} \\ \nabla_{\pmb{\phi}} \leftarrow \nabla_{\pmb{\phi}} + \nabla_{\pmb{\phi}} \, \mathcal{L} \end{array} 
      end for
      \phi \leftarrow \phi - \eta \nabla_{\phi} \{ \text{Update hypernetwork} \}
end for
return \phi
```

3.5 Predicting with iLTM

At inference time, we fix the hypernetwork g_{ϕ^*} obtained from meta-training. Algorithm 2 shows the deployment on a new dataset \mathcal{D} . We first fit a GBDT (or apply robust preprocessing, or both) to obtain embedding parameters γ . Then, we choose a *generation subset* $(X_{\text{gen}}, y_{\text{gen}}) \subset \mathcal{D}_{\text{new}}$ and compute $\tilde{X}_{\text{gen}} = \Psi_{\gamma}(X_{\text{gen}})$. Passing $(\tilde{X}_{\text{gen}}, y_{\text{gen}})$ to the hypernetwork gives θ_{new} , the main-network weights specialized to \mathcal{D}_{new} .

For query points x_* , the model outputs $\hat{y}_* = f_{\theta_{\text{new}}}(\Psi_{\gamma,\omega}(x_*))$. Optionally, one may fine-tune θ_{new} on the training set $\mathcal{D}_{\text{train}}$. We also implement a *retrieval* mechanism (cf. Section 3.2.1), interpolating the main-network output with neighbor-based logits using a temperature τ and weight α . Finally, an ensemble can be obtained by generating multiple $\theta_{\text{new}}^{(m)}$ using different generation subsets or feature bagging, and average their predictions.

Algorithm 2 Inference with iLTM

```
1: Input: Fixed hypernetwork g_{\phi^*}, new dataset \mathcal{D}.

2: Fit GBDT and/or preprocessing on \mathcal{D}_{\text{train}} to obtain \gamma.

3: Select a generation subset (\boldsymbol{X}_{\text{gen}}, \boldsymbol{y}_{\text{gen}}) \subset \mathcal{D}_{\text{train}}.

4: \hat{\boldsymbol{X}}_{\text{gen}}, \ \boldsymbol{\omega} \leftarrow \Psi_{\gamma}(\boldsymbol{X}_{\text{gen}}).

5: \boldsymbol{\theta}_{\text{new}} \leftarrow g_{\phi^*}(\tilde{\boldsymbol{X}}_{\text{gen}}, \boldsymbol{Y}_{\text{gen}}).

6: For any sample \boldsymbol{x}_* \in \mathcal{D}_{\text{test}}: \hat{\boldsymbol{y}}_* \leftarrow f_{\boldsymbol{\theta}_{\text{new}}}\Big(\Psi_{\gamma,\boldsymbol{\omega}}(\boldsymbol{x}_*)\Big).
```

- 7: **Optionally** incorporate retrieval-based predictions with weight α and temperature τ .
- 8: **Optionally** fine-tune θ_{new} with $\mathcal{D}_{\text{train}}$.
- 9: Optionally repeat Steps 3–6 with different (X_{gen}, Y_{gen}) sample or feature subsets to form an ensemble; average predictions.
- 10: return \hat{y}_{new} .

4 Implementation

4.1 Meta-Training Data Collection

We construct a meta-training collection from a large set of approximately 5,000 publicly available classification datasets on OpenML [52], spanning diverse domains such as healthcare, finance, and biology. To prevent overlap with the benchmarks used in our experiments (Section 5.1) and ensure no potential data leakage, we follow strict discarding criteria, fully described in Section C. In brief, we remove any dataset appearing in or highly similar to the evaluation set, exclude duplicates or near-duplicates (by name, shape, or sample-level checks), and discard edge cases. After these steps, we retain 1,806 datasets in our meta-training collection.

4.2 Model

For the embedding stage of the iLTM model (described in detail in Section 3.1), we use random features of dimension $r=2^{15}$ followed by a principal component reduction to dimension $d_{\rm main}=512$ (Section 3.1.2). We also experimented with 1024 dimensions, which caused the pretraining to be way slower, and required a larger GPU with more than 24 GB, and with 256, which worsened the performance significantly. During pre-training we fix the maximum number of boosting rounds in the GBDT embedding to 100, and apply early stopping, which balances expressivity, run-time, and embedding dimension, preventing feature explosion.

The hypernetwork of iLTM is built from MLP blocks with 1024 hidden units, followed by average pooling over the sample dimension to generate each layer's parameters in the main network. The main network $f_{\theta}(\tilde{x})$ is an MLP with 512 hidden units in each layer. We fix a batch size of 2048 for meta-training. This configuration yields strong performance while running in a single A5500 GPU with 24 GB.

4.3 Pre-Training

We follow the meta-training procedure in Algorithm 1 (Section 3.4) on a collection of 1806 tabular datasets. To avoid repeatedly fitting GBDTs online, we train each GBDT (or robust preprocessing) offline for each dataset and cache the resulting transformations. This procedure yields $\Gamma_{\gamma}(\boldsymbol{X}) \in \{0,1\}^{N \times M}$ (if using GBDT embeddings) or the appropriately scaled and encoded features (if using robust preprocessing). We then apply the random features and PCA to obtain $\tilde{\boldsymbol{X}}_{\text{gen}}$.

Although one could refit multiple GBDTs per dataset with different seeds to increase data diversity, we found such augmentation computationally prohibitive. Instead, each dataset is loaded with its fixed embedding during the meta-training loop. Our meta-training runs typically converge within $\sim \! 400\,000$ steps with a gradient accumulation size A=40, after which we select the checkpoint that yields the best meta-validation performance (e.g. few-shot accuracy on held-out datasets).

4.4 Inference

At inference on a new dataset \mathcal{D} , we first fit the chosen embedding Γ_{γ} or robust scaling on $\mathcal{D}_{\text{train}}$. We then choose a generation subset $\{X_{\text{gen}}, y_{\text{gen}}\} \subset \mathcal{D}_{\text{train}}$. For small $\mathcal{D}_{\text{train}}$, we often use all samples; for large $\mathcal{D}_{\text{train}}$, we sample a subset. After mapping X_{gen} to \tilde{X}_{gen} , we feed \tilde{X}_{gen} and y_{gen} into g_{ϕ}^* to generate θ_{new} . Any test point $x_* \in \mathcal{D}_{\text{test}}$ is mapped to \tilde{x}_* and passed through the main network to predict logits $f_{\theta_{\text{new}}}(\tilde{x}_*)$.

We allow a *dynamic* strategy for fitting the GBDT embedding: if the dataset size is under 2 000 samples, we use all training points to fit the GBDT; otherwise, we use a 50% of the training data, up to a maximum size of 100 000 samples, and use the rest to sample the generation sets for the hypernetwork. All GBDTs are trained with early stopping (with 50 rounds without improvement) to mitigate overfitting and reduce run-time. This integrated inference procedure allows iLTM to adapt flexibly to various data scales while preserving strong predictive performance.

Optionally, one may fine-tune θ_{new} on $\mathcal{D}_{\text{train}}$. We also implement feature bagging and multi-subset ensembling by generating multiple $\theta_{\text{new}}^{(m)}$ from different subsets $\{X_{\text{gen}}^{(m)}, y_{\text{gen}}^{(m)}\}$ and averaging their predictions.

5 Benchmarks

5.1 TabZilla Hard Benchmark

To compare iLTM to existing machine learning models for tabular data classification, we evaluate it on the TabZilla Benchmark Suite (TabZilla Hard) [12]. TabZilla comprises 36 datasets specifically selected for their challenging characteristics based on three criteria: (1) baseline-resistant datasets where simple models fail to achieve competitive performance, (2) datasets where only a few algorithms (three or fewer) achieve top performance, and (3) datasets where Gradient Boosting Decision Trees (GBDTs) underperform, ensuring diversity in algorithmic challenges. The entire list of datasets and their dimensions can be found in Appendix B.2.1.

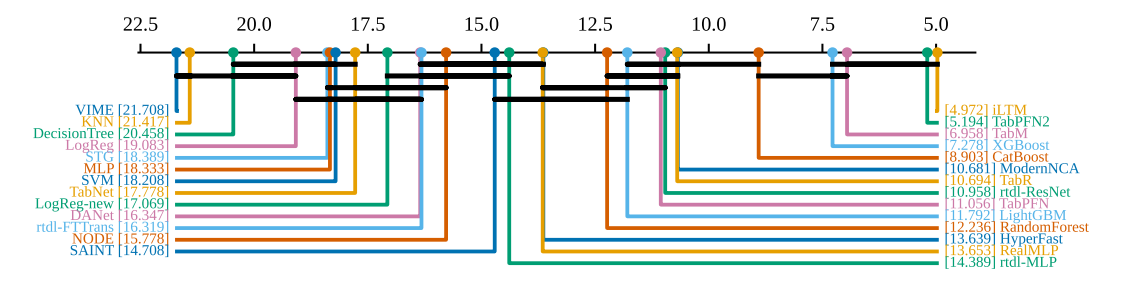


Figure 3: Critical difference diagram [53] of average AUC rankings, showing algorithm groups determined by the Conover post-hoc test [54] following a Friedman test [55] at significance level 0.05. Algorithms connected by a horizontal bar show no statistically significant difference in performance. For algorithms with missing runs, their average rank was imputed using their performance on completed datasets, while those with more than ten missing datasets were removed. Note that iLTM and TabPFNv2 (among others) ran on all datasets.

We follow the TabZilla benchmarking pipeline for both benchmark sets [12], adhering to their test folds, preprocessing steps, and evaluation metrics and constraints. In particular, every model runs one run with default hyperparameter, and 29 additional ones with random hyperparameters. Each run can take up to 2 hours, and all runs cannot surpass more than 10 hours. In contrast to our lightweight GBDT embedding stage, GBDT baselines like XGBoost and CatBoost on tabular benchmarks are typically run with extensive hyperparameter sweeps and, on larger datasets, often fit an order of magnitude more trees than we do.

Using the public results from [12], we compare iLTM with all TabZilla methods that successfully ran on the vast majority of datasets by excluding only methods that failed on 10 or more datasets. The resulting pool of included original baselines is: k-nearest neighbors (KNN) [49], logistic regression [56], decision trees [34], Random Forests [35], SVMs [57], VIME [58], STG [59], TabNet [27], DANets [60], NODE [39], MLP (rtdl-MLP), ResNet (rtdl-ResNet), FT-Transformer (rtdl-FTTrans) [29], SAINT [30], LightGBM [38], TabPFN [15], CatBoost [37], and XGBoost [36]. In addition, we extend the benchmark by introducing several additional baselines; LogReg-new, which extends the original logistic regression setup [56] with a larger hyperparameter search, and several newer methods, namely, HyperFast [16], TabR [20], RealMLP [10], ModernNCA [21], TabM [61], and TabPFNv2 [18]. We note that HyperFast shares several architectural similarities with iLTM and, unlike iLTM, may have been pretrained on datasets that overlap with the benchmark suite. For TabPFN [15], we subset to 30 features that maximize mutual information, select 3000 random samples, and use one-vs-rest classification, as the model does not support larger datasets or more than 10 classes. Similarly, for TabPFNv2 [18], we subset to the maximum supported limit of 500 features and 10,000 samples, and use one-vs-rest for more than 10 classes. The search space for the hyperparameter random search executed by TabZilla for iLTM and all added baselines can be found in Appendix B.3.

Our experimental results demonstrate that iLTM obtains the best mean AUC ranking among all compared methods, as shown in the critical difference diagram (Figure 3). The diagram reveals several statistically indistinguishable groups of algorithms according to the Conover post-hoc test, with iLTM, TabPFNv2, XGBoost, and CatBoost forming the top-performing group. Additional metrics and complete results for the top methods on TabZilla Hard can be found in Appendix B.2.1.

5.2 High-Dimensional Collection Benchmark

For our curated high-dimensional dataset collection, mostly composed of biomedical datasets, we focus our comparison on XGBoost [36] as a close competitor that ran on all the datasets for TabZilla Hard [12]. Note that TabPFNv2 [18] is not designed for large tables, and TabR [20] suffered out-of-memory or time-limit errors on several of the TabZilla Hard datasets that are large. For these experiments, we follow the TabZilla setup with the same compute and time constraints (Section 5.1). Table 1 shows how iLTM maintains its performance advantage on high-dimensional tasks, achieving a higher average AUC compared to XGBoost. The results indicate that iLTM outperforms XGBoost on the majority of the evaluated datasets, with notable improvements on biomedical applications such as SMK-CAN-187 and TOX-171. More details about this benchmarks are available in Section B.1.2.

Dataset	XGBoost	iLTM
CLL-SUB-111	$0.9317_{\pm 0.0516}$	$0.9577_{\pm 0.0405}$
lung	$0.9633_{\pm 0.0644}$	$0.9897_{\pm 0.0182}$
Prostate-GE	$0.9360_{\pm 0.1295}$	$0.8967_{\pm 0.1295}$
SMK-CAN-187	$0.6890_{\pm 0.1779}$	$0.7336_{\pm 0.0943}$
TOX-171	$0.9377_{\pm 0.0277}$	$0.9750_{\pm 0.0269}$
arcene	$0.8921_{\pm 0.0812}$	$0.8831_{\pm 0.0812}$
gisette	$0.9970_{\pm 0.0013}$	$0.9976_{\pm 0.0015}$
Average	$0.9067_{\pm 0.0762}$	$0.9191_{\pm 0.0567}$

Table 1: AUC scores for high-dimensional datasets.

5.3 Transfer to Regression Tasks

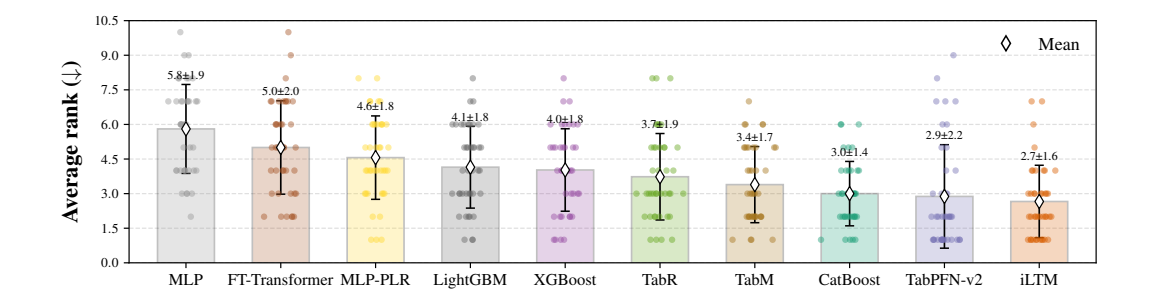


Figure 4: Average rank (\downarrow) on the 18 public regression datasets from [13] also used in [20, 61]. The meta-trained iLTM, fine-tuned on each task, achieves the top overall rank, outperforming gradient-boosted trees and performing on par with recent deep tabular models, illustrating that features learned during classification pretraining transfer effectively to regression problems.

As shown in Fig. 4, despite being pretrained solely on classification corpora, iLTM transfers smoothly to regression problems after short fine-tuning. It obtains the best average rank on the 18 public regression datasets from [13] also used in recent works [20, 61], outperforming GBDT models and recent deep tabular methods like TabM and TabPFNv2. Performance of iLTM drops when starting the fine-tuning of the main network from randomly initialized weights, instead of the weights predicted by the hypernetwork. This indicates that the representations learned during classification pretraining can generalize well across task types, enabling iLTM to deliver state-of-the-art performance with minimal adaptation. More details about the transfer learning to regression are included in Section 6.1 and about the regression benchmark in Section B.

5.4 TabReD Benchmark

Finally, we evaluate iLTM on TabReD [22], a benchmark with industry-grade tabular datasets and time-based splits that includes both classification and regression tasks. We include models used in real-world production settings that can scale to the size of the TabReD datasets [62, 63], classical GBDT models [36, 37, 38], MLP-based models [29, 64, 65, 66, 61], a Transformer-based method [29], and a retrieval-based method [20]. iLTM obtains very competitive results and surpasses GBDT-only methods and recent deep tabular baselines, on both regression and classification tasks, obtaining the best average rank across the 8 tasks.

Table 2: TabReD classification and regression benchmarks (mean \pm std) performance comparison.

	Classif	fication (ROC	AUC ↑)		Regression (RMSE \downarrow)			Average	
Methods	Homesite Insurance	Ecom Offers	HomeCredit Default	Sberbank Housing	Cooking Time	Delivery ETA	Maps Routing	Weather	Rank↓
Non DL Baselines XGBoost [36] LightGBM [38] CatBoost [37]	$\begin{array}{c} 0.960_{\pm 0.000} \\ 0.960_{\pm 0.000} \\ 0.961_{\pm 0.000} \end{array}$	$0.576_{\pm 0.001}$	$\begin{array}{c} 0.867_{\pm 0.001} \\ 0.866_{\pm 0.000} \\ 0.862_{\pm 0.001} \end{array}$	$\begin{array}{c} 0.242_{\pm 0.001} \\ 0.247_{\pm 0.001} \\ 0.248_{\pm 0.003} \end{array}$	$\begin{array}{c} 0.482_{\pm 0.000} \\ 0.483_{\pm 0.000} \\ 0.482_{\pm 0.000} \end{array}$	$\begin{array}{c} 0.547_{\pm 0.000} \\ 0.547_{\pm 0.000} \\ 0.546_{\pm 0.000} \end{array}$	$\begin{array}{c} 0.162_{\pm 0.000} \\ 0.162_{\pm 0.000} \\ 0.162_{\pm 0.000} \end{array}$	$\begin{array}{c} 1.467_{\pm 0.001} \\ 1.462_{\pm 0.001} \\ 1.469_{\pm 0.002} \end{array}$	$2.9_{\pm 1.6}$ $3.3_{\pm 1.6}$ $3.6_{\pm 1.4}$
Tabular DL Models MLP [29] SNN [64] DFR [65] DCNv2 [62] ResNet [29] FT-Transformer [29] MLP-PLR [66] TabR [20] TabM [61]	$\begin{array}{c} 0.950_{\pm 0.000} \\ 0.949_{\pm 0.002} \\ 0.950_{\pm 0.000} \\ 0.939_{\pm 0.006} \\ 0.947_{\pm 0.002} \\ 0.962_{\pm 0.001} \\ 0.962_{\pm 0.000} \\ 0.949_{\pm 0.001} \\ 0.964_{\pm 0.000} \end{array}$	$\begin{array}{c} 0.600_{\pm 0.003} \\ 0.601_{\pm 0.001} \\ 0.596_{\pm 0.007} \\ 0.600_{\pm 0.004} \\ 0.578_{\pm 0.006} \\ 0.596_{\pm 0.003} \\ 0.594_{\pm 0.002} \end{array}$	$\begin{array}{c} 0.855{\scriptstyle \pm 0.001} \\ 0.855{\scriptstyle \pm 0.001} \\ 0.855{\scriptstyle \pm 0.001} \\ 0.847{\scriptstyle \pm 0.003} \\ 0.849{\scriptstyle \pm 0.003} \\ 0.857{\scriptstyle \pm 0.002} \\ 0.857{\scriptstyle \pm 0.001} \\ 0.850{\scriptstyle \pm 0.003} \\ 0.860{\scriptstyle \pm 0.001} \end{array}$	$\begin{array}{c} 0.251_{\pm 0.005} \\ 0.286_{\pm 0.045} \\ 0.249_{\pm 0.004} \\ 0.277_{\pm 0.016} \\ 0.274_{\pm 0.034} \\ 0.244_{\pm 0.004} \\ 0.242_{\pm 0.005} \\ 0.282_{\pm 0.032} \\ 0.244_{\pm 0.002} \end{array}$	$\begin{array}{c} 0.482_{\pm 0.000} \\ 0.484_{\pm 0.001} \\ 0.482_{\pm 0.000} \\ 0.484_{\pm 0.001} \\ 0.482_{\pm 0.000} \\ 0.482_{\pm 0.001} \\ 0.483_{\pm 0.001} \\ 0.480_{\pm 0.000} \end{array}$	$\begin{array}{c} 0.550_{\pm 0.001} \\ 0.554_{\pm 0.003} \\ 0.551_{\pm 0.000} \\ 0.553_{\pm 0.002} \\ 0.553_{\pm 0.002} \\ 0.554_{\pm 0.003} \\ 0.553_{\pm 0.002} \\ 0.551_{\pm 0.002} \\ 0.549_{\pm 0.000} \end{array}$	$\begin{array}{c} 0.162 {\pm} 0.000 \\ 0.165 {\pm} 0.001 \\ 0.163 {\pm} 0.000 \\ 0.167 {\pm} 0.001 \\ 0.163 {\pm} 0.000 \\ 0.163 {\pm} 0.000 \\ 0.162 {\pm} 0.000 \\ 0.164 {\pm} 0.000 \\ 0.161 {\pm} 0.000 \\ 0.161 {\pm} 0.000 \end{array}$	$\begin{array}{c} 1.547_{\pm 0.004} \\ 1.565_{\pm 0.009} \\ 1.551_{\pm 0.004} \\ 1.578_{\pm 0.006} \\ 1.502_{\pm 0.004} \\ 1.510_{\pm 0.010} \\ 1.518_{\pm 0.006} \\ 1.467_{\pm 0.004} \\ 1.472_{\pm 0.002} \end{array}$	$\begin{array}{c} 4.6 \pm 2.1 \\ 6.3 \pm 2.1 \\ 5.0 \pm 2.3 \\ 7.1 \pm 2.5 \\ 5.5 \pm 1.9 \\ 4.6 \pm 1.7 \\ 3.6 \pm 1.8 \\ 5.4 \pm 2.1 \\ 2.6 \pm 1.5 \end{array}$
iLTM (Ours)	$0.961_{\pm0.000}$		$0.865_{\pm0.001}$	$0.237_{\pm 0.001}$	$0.482_{\pm 0.001}$	$0.548_{\pm0.002}$	$0.162_{\pm0.000}$	$1.464_{\pm0.004}$	2.5 ± 0.9

6 Analysis

6.1 Transfer to Regression

To apply iLTM to regression tasks, the same architecture is used and per-class operations become dataset-level where needed. After the initial transformation, we compute the global mean of the transformed features over the batch, replacing the per-class means used in classification. The standardized target y of the batch is passed to the hypernetwork, instead of a one-hot label tensor. The hypernetwork block processes the embeddings exactly as in classification, generating a set of layer weights. For the final prediction layer, the per-sample weight predictions are averaged to obtain a single weight vector, which is reshaped into a linear mapping that produces the regression output.

Table 3: Performance (RMSE) improvement and fine-tuning time of iLTM compared to starting from random initialization.

Configuration	Improvement	Time (s)
Main network from random init. (baseline) Main network from hypernetwork (transfer)	$^{-}$ 46.2% \pm 8.4%	47.151 ± 9.502 24.348 ± 5.961
Main network from hypernetwork (transfer) + ensembling ($\times 5$)	$51.0\% \pm 7.4\%$	97.271 ± 25.467

To obtain accurate predictions for regression, some fine-tuning steps are required because the hypernetwork was pretrained on classification tasks. Table 3 shows the average performance improvement when using the weights generated by iLTM and fine-tuning for regression tasks, compared to randomly initializing the linear layers (no use of the pretrained hypernetwork) on the validation set of 5 datasets from [20] (california, diamond, isolet, analcatdata supreme, fifa). Not only is improvement significant, but fine-tuning time is halved compared to training from scratch. Ensembling further boosts performance, and training five predictors only doubles the time relative to a single randomly initialized network, effectively showing that large-scale pretraining on classification transfers to regression tasks.

6.2 Weight Space Analysis

We explore the structure of the weight space induced by our meta-trained hypernetwork and the main networks it produces for different tasks. The weight vectors $\boldsymbol{\theta}$ produced by the hypernetwork can be regarded as points in a high-dimensional weight space $\boldsymbol{\Theta}$. Recent works [67, 68] have studied the weight space of populations of neural networks, providing insights into model characteristics, downstream tasks behavior, and generative modeling. In our framework, the meta-trained hypernetwork learns dataset-level embeddings, which uses to produce populations of neural networks for multiple tasks in a shared weight space.

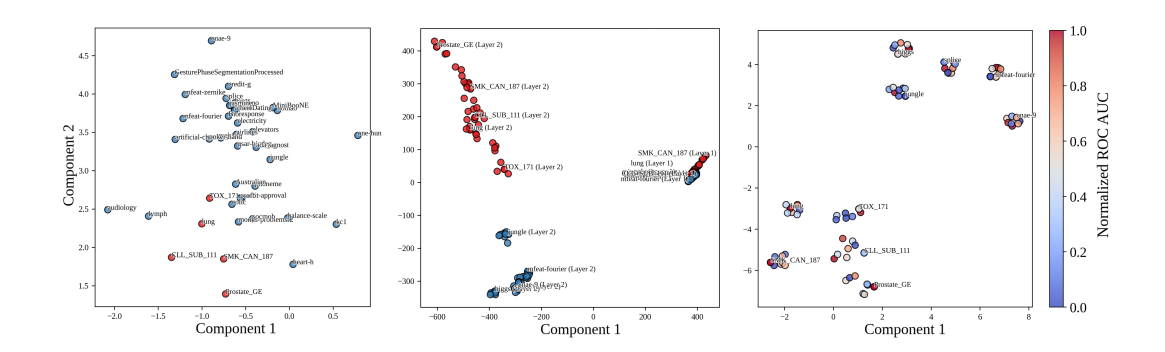


Figure 5: Left: t-SNE of concatenated hypernetwork embeddings across all three layers in embedding space, with blue and red points represent Tabzilla Hard and high dimensional biomedical datasets, respectively. Center: PCA of weights from 8 ensemble predictors trained on each dataset, showing the first two layers separately in weight space. Right: t-SNE of the weights from the 8 predictors, with weights concatenated across all three layers in weight space, colored by normalized AUC.

In Figure 5, we visualize this structure on a representative subset of datasets. On the left, we show a t-SNE visualization [69] of concatenated *hypernetwork representations* (*i.e.*, the dataset-level hyper-representations obtained by the hypernetwork before generating the weights) across all three main layers. The embeddings for tasks from the same domain naturally cluster together, indicating that the hypernetwork has learned to generate similar internal representations for datasets sharing certain characteristics. Notably, the high-dimensional biomedical tasks (in red) form a cluster that is also close to health-related datasets from TabZilla Hard (in blue), *i.e.*, *audiology*, *lymph*, *colic*, and *heart-h*, reflecting domain-level similarities. The center plot shows PCA applied to weights of the first two layers produced by eight different predictors generated for each dataset. The first layer generated by the hypernetwork shows less variance, as it captures more generic representations across datasets, while the second tends to vary more from one dataset to another, probably learning higher-level representations adapted to each task. The right plot depicts the weight vectors colored by normalized ROC AUC per dataset, and concatenated for all layers, which cluster for each dataset.

To better understand how these task-specific weights evolve during fine-tuning, Figure 6 illustrates trajectories of four ensemble predictors on the *jungle-chess* dataset, part of TabZilla Hard. In Fig. 6a, although all predictors begin from closely related initializations generated by the hypernetwork, they diverge over fine-tuning. Displaying distinct trajectories in the two dominant principal components, they gradually become more dissimilar in weight space and thereby increase predictor diversity, a phenomenon beneficial for ensembling, as diversified predictors capture complementary aspects of the data [70, 71]. In Fig. 6b, the corresponding ROC AUC increases steadily for each predictor, confirming that the weight trajectories move toward solutions of higher predictive performance. In Fig. 6c, the average inter-predictor variance rises as fine-tuning progresses, indicating again that the ensemble members become more diverse.

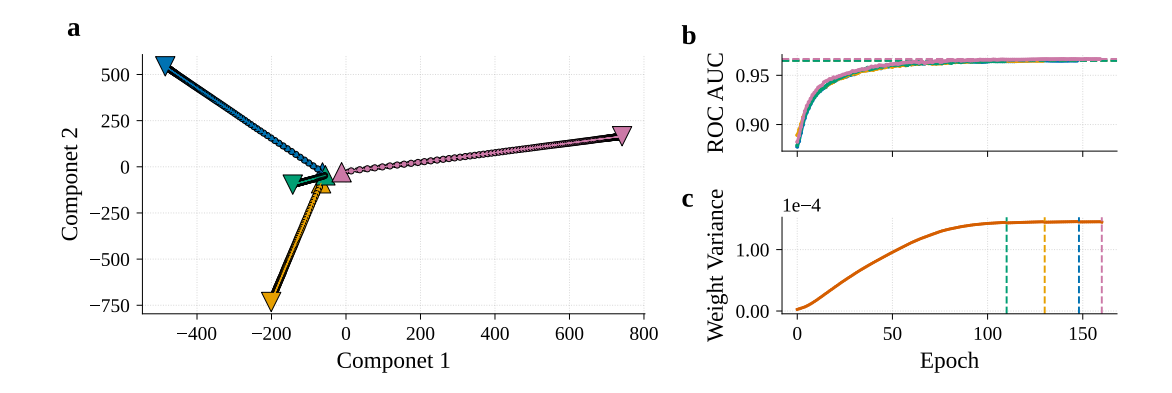


Figure 6: Visualization of finetuning on the *jungle-chess* dataset. (a) Evolution of model weights projected onto the first two principal components, with colors for each of four ensemble predictors; triangles indicate start (\blacktriangle) and end (\blacktriangledown), larger points are epoch boundaries, and smaller points, intermediate iterations. (b) AUC across epochs, with dashed lines showing each predictor's final performance. (c) Variance of weights across predictors over epochs, with vertical dashed lines marking each predictor's finetuning completion by early stopping.

6.3 Few-Shot Meta-Validation Analysis

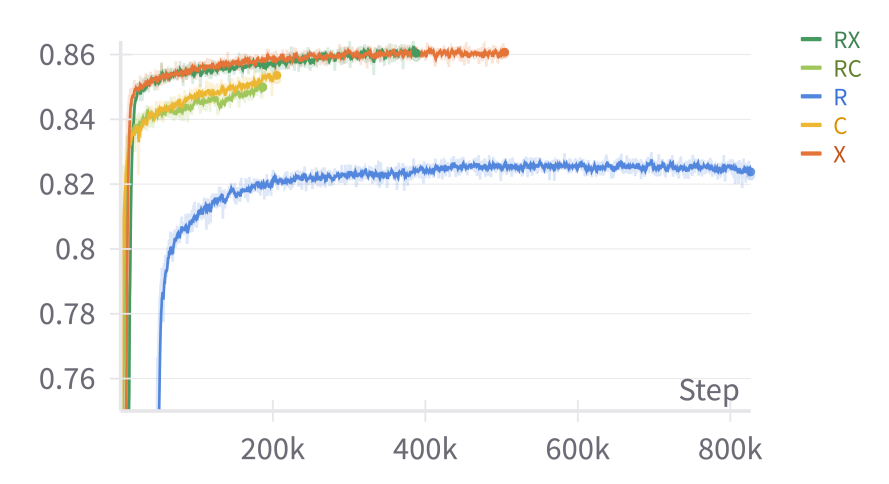


Figure 7: Average few-shot meta-validation AUC for each preprocessing: R (robust without GBDT), X (XGBoost-based), C (CatBoost-based), and the concatenations RX and RC.

Figure 7 compares performance across five preprocessing configurations during meta-validation in pre-training. Because R-only runs complete each training step more quickly, they can accumulate the highest number of updates in the seven-day limit, with X next in throughput and C the slowest. Including GBDT embeddings (X or C) yields higher few-shot accuracy early on—an effect clearly visible when validating on a single batch without fine-tuning—yet this comes at the cost of slower iteration. Concatenations RX and RC also show similarly high few-shot gains, but run marginally slower than single-embedding configurations, as they process both sets of features. Notably, GBDT-based embeddings provide a strong initialization for new tasks, which helps explain their advantage in a few-shot setting. Nonetheless, once full fine-tuning is allowed over one whole dataset during inference, R-only can match or even surpass the X- and C-based variants despite its initially lower few-shot performance.

6.4 Ablation Study

This section presents an ablation study to demonstrate the effectiveness of the different components of iLTM. The experiments are conducted on the *cylinder-bands*, *ecoli*, *connect-4*, *christine*, and *volkert* datasets from OpenML [72], selected for their varied dimensions. The pre-specified data folds are used for evaluation, and all executions are performed on a single NVIDIA A5500 GPU.

How Effective Is the Pre-Trained Hypernetwork? To evaluate the effectiveness of the pre-trained hypernetwork within the iLTM framework, Table 4 presents a comparative performance analysis. We examine three configurations: the main network whose weights are generated by iLTM's hypernetwork in a single forward pass from a batch of data, the iLTM-generated main network with subsequent fine-tuning with early stopping on the complete training set, and a main network with randomly initialized weights trained from scratch with early stopping on the complete training set, representing a standard training approach without leveraging iLTM's hypernetwork. The performance is assessed based on AUC, fit time (in seconds), and prediction time (in seconds).

Table 4: Performance comparison demonstrating the effectiveness of the iLTM hypernetwork. Values represent mean \pm standard deviation.

Configuration	AUC	Fit time (s)	Predict time (s)
Training from random weights on all data	$0.826_{\pm0.167}$	$94.013_{\pm 247.115}$	$0.969_{\pm0.810}$
iLTM base (one forward pass on one batch) iLTM + fine-tuning on all data	$\begin{array}{c} 0.803_{\pm 0.129} \\ 0.856_{\pm 0.134} \end{array}$	$3.292_{\pm 3.588}$ $27.229_{\pm 32.830}$	$0.955_{\pm 0.802} \\ 0.949_{\pm 0.791}$

The results presented in Table 4 clearly demonstrate the significant advantages of employing the pre-trained hypernetwork in iLTM.

Regarding AUC performance, the iLTM with fine-tuning configuration achieves the highest AUC, outperforming the standard approach of training a neural network from scratch. This indicates that the hypernetwork provides a superior weight initialization, leading to a better final model after fine-tuning. Even the configuration using iLTM without finetuning yields a respectable AUC. While lower than the fine-tuned models, this result highlights that the hypernetwork can generate reasonably effective main network weights directly.

In terms of fit time, the most striking benefit is observed. iLTM base is exceptionally fast, as it only requires a single forward pass on one batch of data through the hypernetwork to generate the main network's weights. Crucially, when addining fine-tuning, it also requires significantly less time to converge compared to training from random weights. The large standard deviation in fit time for training from weights initialization also suggests that training from scratch can be more variable and potentially prone to longer convergence times depending on the initialization and data.

Finally, prediction times are comparable across all three configurations. This is expected, as the underlying architecture of the main network used for inference is the same, regardless of how its weights were obtained.

In conclusion, these findings underscore that the hypernetwork in iLTM provides a dual advantage: it initializes the main network with weights that lead to higher AUC after fine-tuning compared to random initialization, and it dramatically reduces the fit time needed to achieve optimal or near-optimal performance, making the training process significantly more efficient. These findings highlight the value of the hypernetwork as a core component of iLTM, enabling both faster and more effective model generation.

Effectiveness of Key Hyperparameters Tables 5, 6, and 7 present an ablation study evaluating the impact of key iLTM hyperparameters on AUC, fit time, and prediction time, respectively. Namely, they present the performance for a single forward pass on one batch of data (Base), and when adding ensembling of 4 predictors (E), retrieval-augmented classification (R), and fine-tuning of the main network on the full training set (F).

Generally, each additional component tends to improve the AUC score. However, as discussed in the introduction, the efficacy of certain techniques can be dataset-dependent. Consequently, some

datasets derive greater benefit from incorporating retrieval or specific embedding strategies (Robust vs. GBDT) than others. Notably, fine-tuning consistently yields the most significant AUC gains.

Regarding fit time, ensembling (x4) leads to an approximately four-fold increase, scaling linearly with the number of predictors. The addition of retrieval incurs a negligible increase in fit time. Fine-tuning, while delivering substantial AUC improvements, also results in the most considerable increase in fit time. Furthermore, the robust embedding requires less time than the GBDT embedding, as it bypasses the need to train a GBDT model and does not expand the input dimensionality.

For prediction time, ensembling (x4) similarly introduces a significant cost, scaling with the number of predictors. In contrast, once an ensemble is in place, the subsequent additions of retrieval and fine-tuning have a relatively minor impact on the overall prediction time.

Table 5: Ablation study on the AUC for serveral iLTM configurations. Base: single predictor, E: ensembling (4 predictors), R: retrieval-augmented, F: fine-tuning. Results shown for Robust preprocessing and GBDT embeddings.

Configuration	Robust	GBDT
Base	$0.859_{\pm 0.083}$	$0.808_{\pm 0.043}$
+ E	$0.866_{\pm 0.077}$	$0.838_{\pm 0.067}$
+ E + R	$0.855_{\pm 0.081}$	$0.853_{\pm 0.091}$
+E+R+F	$0.927_{\pm 0.060}$	$0.896_{\pm 0.073}$

Table 6: Ablation study on the fit time (in seconds) for serveral iLTM configurations. Base: single predictor, E: ensembling (4 predictors), R: retrieval-augmented, F: fine-tuning. Results shown for Robust preprocessing and GBDT embeddings.

Configuration	Robust	GBDT
Base	$2.896_{\pm 2.308}$	$7.556_{\pm 2.545}$
+ E	$6.404_{\pm 3.596}$	$13.813_{\pm 4.467}$
+E+R	$6.134_{\pm 3.763}$	$13.592_{\pm 4.349}$
+E+R+F	$263.111_{\pm 309.644}$	$313.517_{\pm 380.552}$

Table 7: Ablation study on the prediction time (in seconds) for serveral iLTM configurations. Base: single predictor, E: ensembling (4 predictors), R: retrieval-augmented, F: fine-tuning. Results shown for Robust preprocessing and GBDT embeddings.

Configuration	Robust	GBDT
Base	$0.719_{\pm 0.258}$	$0.929_{\pm 0.246}$
+ E	$2.540_{\pm 0.381}$	$3.367_{\pm0.820}$
+ E + R	$2.563_{\pm 0.541}$	$3.679_{\pm 1.204}$
+ E + R + F	$2.519_{\pm 0.462}$	$3.714_{\pm 1.155}$

7 Discussion

We introduce iLTM, a large tabular model that integrates tree-based representations, meta-learned hypernetworks, and deep neural architectures with retrieval-augmented predictions into a single model that yields strong and reliable performance across a diverse range of tabular tasks. By incorporating gradient-boosted decision-tree embeddings, our method inherits the robust inductive biases that have long made tree ensembles the preferred choice for many real-world tabular problems [35, 36, 37, 38, 5, 13]. At the same time, the hypernetwork-based MLP backbone and retrieval module provide a scalable and expressive framework that benefits from large-scale meta-training while remaining flexible enough to adapt quickly to new tasks, and they connect to retrieval-augmented modeling that has proven effective in other domains and in tabular settings [20, 21]. Crucially, our experiments demonstrate that this neural-tree hybrid approach not only matches but surpasses GBDTs

and well-tuned neural baselines, minimally tuning the GBDT embedding, suggesting that both the tree-based and neural paradigms contribute complementary strengths within the iLTM architecture.

Strong performance of iLTM spans very different tabular distributions and scales. On relatively small datasets with mixed feature types, GBDT embeddings effectively capture discrete feature interactions, which are then refined by the MLP. Meanwhile, in large and high-dimensional settings, iLTM's neural capacity and retrieval mechanism allow it to scale more gracefully than methods that rely on massive ensembles or carefully tuned attention blocks [29, 28]. This adaptability partly arises from the meta-trained hypernetwork, which internalizes knowledge from a large and varied corpus of tabular datasets. By distilling patterns that frequently arise across heterogeneous tasks, the hypernetwork can generate MLP weights that give a favorable initialization, requiring minimal fine-tuning at test time. The weight space analysis (Section 6.2) shows that iLTM's hypernetwork both captures meaningful global structure clustering different tasks by domain and provides flexible local search directions that fine-tuning can exploit. iLTM ensemble members start from different meta-learned weights and sample different batches, producing models with greater diversity that benefit more from ensembling. The results also suggests the potential for future work on combining or interpolating models in this space to balance specialization and generalization across tasks. While standard GBDTs often demand fresh hyperparameter searches for each new dataset, iLTM amortizes the effort of meta-training, cutting down the hyperparameter optimization for the GBDT part, and deployment time without sacrificing predictive accuracy. Further experiments and insights on few-shot performance of iLTM, ablations, and high-dimensional data are provided in the Supplementary Information.

From a practical standpoint, the inclusion of GBDT embeddings introduces an additional step that might add overhead relative to a purely neural pipeline. In practice, however, the overall meta-trained workflow remains efficient because GBDT training and embedding generation are performed once per dataset, after which hypernetwork inference is rapid. Moreover, as the embeddings map tabular features into a structured sparse binary format, the MLP can more readily learn irregular functions without first having to discover relevant patterns.

Being pretrained exclusively on classification tasks, iLTM shows strong transfer learning capabilities on regression tasks, but performance on other out-of-distribution tasks could be limited. Second, fitting a GBDT for every new dataset introduces an extra processing stage that can be prohibitive in latency-critical scenarios. However, this step is optional, and the robust preprocessing can be used without fitting any GBDT. Finally, the retrieval module employs a fixed similarity metric; when the feature distribution drifts, this static metric can select sub-optimal neighbors, limiting the benefits of retrieval-augmented inference [22].

Future directions could explore extending the meta-training corpus to include regression and other tasks to broaden the model's inductive biases. Making the retrieval component more dynamic by learning an adaptive similarity metric might further improve accuracy on niche domains where local neighborhoods offer important information, e.g. precision health or finance. Incorporating lightweight attention blocks directly into the main network could enhance the capture of higher-order interactions not explicitly represented in tree splits. Finally, further probing the internal structure of the hypernetwork-generated weight space $\theta \in \Theta$ [68] may provide deeper insights into how iLTM generalizes across tasks and inform both compression and interpretability efforts.

Overall, the results advocate for a paradigm shift that unifies traditionally separate lines of research in tabular learning. By demonstrating that tree embeddings, meta-learning, and deep neural methods can be fused into a cohesive *foundation model* approach, iLTM paves the way for future tabular models that seamlessly adapt to a wide array of settings with limited tuning, bridging the gap between specialized methods for small, structured datasets and the large-scale neural approaches that dominate other domains.

Acknowledgements

MCC was supported by a fellowship from "la Caixa" Foundation (ID 100010434, code B006360) during part of the development of this project.

References

- [1] Tom Brown, Benjamin Mann, Nick Ryder, Melanie Subbiah, Jared D Kaplan, Prafulla Dhariwal, Arvind Neelakantan, Pranav Shyam, Girish Sastry, Amanda Askell, et al. Language models are few-shot learners. *Advances in neural information processing systems*, 33:1877–1901, 2020.
- [2] Robin Rombach, Andreas Blattmann, Dominik Lorenz, Patrick Esser, and Björn Ommer. High-resolution image synthesis with latent diffusion models. In *Proceedings of the IEEE/CVF conference on computer vision and pattern recognition*, pages 10684–10695, 2022.
- [3] Alec Radford, Jong Wook Kim, Chris Hallacy, Aditya Ramesh, Gabriel Goh, Sandhini Agarwal, Girish Sastry, Amanda Askell, Pamela Mishkin, Jack Clark, et al. Learning transferable visual models from natural language supervision. In *International conference on machine learning*, pages 8748–8763. PMLR, 2021.
- [4] Weizheng Lu, Jing Zhang, Ju Fan, Zihao Fu, Yueguo Chen, and Xiaoyong Du. Large language model for table processing: A survey. *Frontiers of Computer Science*, 19(2):192350, 2025.
- [5] Vadim Borisov, Tobias Leemann, Kathrin Seßler, Johannes Haug, Martin Pawelczyk, and Gjergji Kasneci. Deep neural networks and tabular data: A survey. *IEEE transactions on neural networks and learning systems*, 2022.
- [6] Han-Jia Ye, Si-Yang Liu, Hao-Run Cai, Qi-Le Zhou, and De-Chuan Zhan. A closer look at deep learning on tabular data. *arXiv preprint arXiv:2407.00956*, 2024.
- [7] Tuan Dinh, Yuchen Zeng, Ruisu Zhang, Ziqian Lin, Michael Gira, Shashank Rajput, Jy-yong Sohn, Dimitris Papailiopoulos, and Kangwook Lee. Lift: Language-interfaced fine-tuning for non-language machine learning tasks. Advances in Neural Information Processing Systems, 35:11763–11784, 2022.
- [8] Stefan Hegselmann, Alejandro Buendia, Hunter Lang, Monica Agrawal, Xiaoyi Jiang, and David Sontag. Tabllm: Few-shot classification of tabular data with large language models. In International Conference on Artificial Intelligence and Statistics, pages 5549–5581. PMLR, 2023.
- [9] Boris van Breugel and Mihaela van der Schaar. Position: Why tabular foundation models should be a research priority. In *Forty-first International Conference on Machine Learning*, 2024.
- [10] David Holzmüller, Leo Grinsztajn, and Ingo Steinwart. Better by default: Strong pre-tuned MLPs and boosted trees on tabular data. In *The Thirty-eighth Annual Conference on Neural Information Processing Systems*, 2024.
- [11] Arlind Kadra, Marius Lindauer, Frank Hutter, and Josif Grabocka. Well-tuned simple nets excel on tabular datasets. *Advances in neural information processing systems*, 34:23928–23941, 2021.
- [12] Duncan McElfresh, Sujay Khandagale, Jonathan Valverde, Vishak Prasad C, Ganesh Ramakrishnan, Micah Goldblum, and Colin White. When do neural nets outperform boosted trees on tabular data? *Advances in Neural Information Processing Systems*, 36, 2024.
- [13] Léo Grinsztajn, Edouard Oyallon, and Gaël Varoquaux. Why do tree-based models still outperform deep learning on typical tabular data? *Advances in neural information processing systems*, 35:507–520, 2022.
- [14] Ravid Shwartz-Ziv and Amitai Armon. Tabular data: Deep learning is not all you need. In 8th ICML Workshop on Automated Machine Learning (AutoML), 2021.
- [15] Noah Hollmann, Samuel Müller, Katharina Eggensperger, and Frank Hutter. TabPFN: A transformer that solves small tabular classification problems in a second. In *The Eleventh International Conference on Learning Representations*, 2023.
- [16] David Bonet, Daniel Mas Montserrat, Xavier Giró-i Nieto, and Alexander G Ioannidis. Hyperfast: Instant classification for tabular data. *Proceedings of the AAAI Conference on Artificial Intelligence*, 38(10):11114–11123, 2024.

- [17] Andreas C Mueller, Carlo A Curino, and Raghu Ramakrishnan. Mothernet: Fast training and inference via hyper-network transformers. In *NeurIPS 2024 Third Table Representation Learning Workshop*, 2024.
- [18] Noah Hollmann, Samuel Müller, Lennart Purucker, Arjun Krishnakumar, Max Körfer, Shi Bin Hoo, Robin Tibor Schirrmeister, and Frank Hutter. Accurate predictions on small data with a tabular foundation model. *Nature*, 637(8045):319–326, 2025.
- [19] Alec Radford, Jong Wook Kim, Tao Xu, Greg Brockman, Christine McLeavey, and Ilya Sutskever. Robust speech recognition via large-scale weak supervision. In *International conference on machine learning*, pages 28492–28518. PMLR, 2023.
- [20] Yury Gorishniy, Ivan Rubachev, Nikolay Kartashev, Daniil Shlenskii, Akim Kotelnikov, and Artem Babenko. Tabr: Tabular deep learning meets nearest neighbors. In *The Twelfth International Conference on Learning Representations*, 2024.
- [21] Han-Jia Ye, Huai-Hong Yin, and De-Chuan Zhan. Modern neighborhood components analysis: A deep tabular baseline two decades later, 2024.
- [22] Ivan Rubachev, Nikolay Kartashev, Yury Gorishniy, and Artem Babenko. Tabred: Analyzing pit-falls and filling the gaps in tabular deep learning benchmarks. arXiv preprint arXiv:2406.19380, 2024.
- [23] Bingzhao Zhu, Xingjian Shi, Nick Erickson, Mu Li, George Karypis, and Mahsa Shoaran. Xtab: cross-table pretraining for tabular transformers. In *Proceedings of the 40th International Conference on Machine Learning*, pages 43181–43204, 2023.
- [24] Myung Jun Kim, Leo Grinsztajn, and Gael Varoquaux. CARTE: Pretraining and transfer for tabular learning. In *Forty-first International Conference on Machine Learning*, 2024.
- [25] Boris van Breugel, Jonathan Crabbé, Rob Davis, and Mihaela van der Schaar. Latable: Towards large tabular models. arXiv preprint arXiv:2406.17673, 2024.
- [26] Jaehyun Nam, Jihoon Tack, Kyungmin Lee, Hankook Lee, and Jinwoo Shin. STUNT: Few-shot tabular learning with self-generated tasks from unlabeled tables. In *The Eleventh International Conference on Learning Representations*, 2023.
- [27] Sercan Ö Arik and Tomas Pfister. Tabnet: Attentive interpretable tabular learning. *Proceedings of the AAAI conference on artificial intelligence*, 35(8):6679–6687, 2021.
- [28] Xin Huang, Ashish Khetan, Milan Cvitkovic, and Zohar Karnin. Tabtransformer: Tabular data modeling using contextual embeddings. *arXiv preprint arXiv:2012.06678*, 2020.
- [29] Yury Gorishniy, Ivan Rubachev, Valentin Khrulkov, and Artem Babenko. Revisiting deep learning models for tabular data. Advances in Neural Information Processing Systems, 34:18932– 18943, 2021.
- [30] Gowthami Somepalli, Micah Goldblum, Avi Schwarzschild, C Bayan Bruss, and Tom Goldstein. Saint: Improved neural networks for tabular data via row attention and contrastive pre-training. *arXiv preprint arXiv:2106.01342*, 2021.
- [31] Yunfan Gao, Yun Xiong, Xinyu Gao, Kangxiang Jia, Jinliu Pan, Yuxi Bi, Yi Dai, Jiawei Sun, and Haofen Wang. Retrieval-augmented generation for large language models: A survey. *arXiv* preprint arXiv:2312.10997, 2023.
- [32] Alexander Long, Wei Yin, Thalaiyasingam Ajanthan, Vu Nguyen, Pulak Purkait, Ravi Garg, Alan Blair, Chunhua Shen, and Anton van den Hengel. Retrieval augmented classification for long-tail visual recognition. In *Proceedings of the IEEE/CVF conference on computer vision and pattern recognition*, pages 6959–6969, 2022.
- [33] Léon Bottou and Vladimir Vapnik. Local learning algorithms. *Neural Computation*, 4(6):888–900, 11 1992.
- [34] J. Ross Quinlan. Induction of decision trees. *Machine learning*, 1(1):81–106, 1986.

- [35] Leo Breiman. Random forests. *Machine learning*, 45:5–32, 2001.
- [36] Tianqi Chen and Carlos Guestrin. Xgboost: A scalable tree boosting system. In *Proceedings of the 22nd acm sigkdd international conference on knowledge discovery and data mining*, pages 785–794, 2016.
- [37] Liudmila Prokhorenkova, Gleb Gusev, Aleksandr Vorobev, Anna Veronika Dorogush, and Andrey Gulin. Catboost: unbiased boosting with categorical features. *Advances in neural information processing systems*, 31, 2018.
- [38] Guolin Ke, Qi Meng, Thomas Finley, Taifeng Wang, Wei Chen, Weidong Ma, Qiwei Ye, and Tie-Yan Liu. Lightgbm: A highly efficient gradient boosting decision tree. *Advances in neural information processing systems*, 30, 2017.
- [39] Sergei Popov, Stanislav Morozov, and Artem Babenko. Neural oblivious decision ensembles for deep learning on tabular data. In *International Conference on Learning Representations*, 2020.
- [40] Guolin Ke, Zhenhui Xu, Jia Zhang, Jiang Bian, and Tie-Yan Liu. Deepgbm: A deep learning framework distilled by gbdt for online prediction tasks. In *Proceedings of the 25th ACM SIGKDD International Conference on Knowledge Discovery & Data Mining*, pages 384–394, 2019.
- [41] Liran Katzir, Gal Elidan, and Ran El-Yaniv. Net-dnf: Effective deep modeling of tabular data. In *International conference on learning representations*, 2020.
- [42] Kuan-Yu Chen, Ping-Han Chiang, Hsin-Rung Chou, Chih-Sheng Chen, and Tien-Hao Chang. DOFEN: Deep oblivious forest ENsemble. In *The Thirty-eighth Annual Conference on Neural Information Processing Systems*, 2024.
- [43] Sascha Marton, Stefan Lüdtke, Christian Bartelt, and Heiner Stuckenschmidt. Grande: Gradient-based decision tree ensembles for tabular data. In *The Twelfth International Conference on Learning Representations*, 2024.
- [44] Xinran He, Junfeng Pan, Ou Jin, Tianbing Xu, Bo Liu, Tao Xu, Yanxin Shi, Antoine Atallah, Ralf Herbrich, Stuart Bowers, et al. Practical lessons from predicting clicks on ads at facebook. In *Proceedings of the eighth international workshop on data mining for online advertising*, pages 1–9, 2014.
- [45] Frank Moosmann, Bill Triggs, and Frederic Jurie. Fast discriminative visual codebooks using randomized clustering forests. *Advances in neural information processing systems*, 19, 2006.
- [46] Ali Rahimi and Benjamin Recht. Random features for large-scale kernel machines. *Advances in neural information processing systems*, 20, 2007.
- [47] Youngmin Cho and Lawrence Saul. Kernel methods for deep learning. *Advances in neural information processing systems*, 22, 2009.
- [48] David Lopez-Paz, Suvrit Sra, Alex Smola, Zoubin Ghahramani, and Bernhard Schölkopf. Randomized nonlinear component analysis. In *International conference on machine learning*, pages 1359–1367. PMLR, 2014.
- [49] Thomas Cover and Peter Hart. Nearest neighbor pattern classification. *IEEE transactions on information theory*, 13(1):21–27, 1967.
- [50] Jacob Goldberger, Geoffrey E Hinton, Sam Roweis, and Russ R Salakhutdinov. Neighbourhood components analysis. *Advances in neural information processing systems*, 17, 2004.
- [51] David Ha, Andrew M. Dai, and Quoc V. Le. Hypernetworks. In *International Conference on Learning Representations*, 2017.
- [52] Matthias Feurer, Jan N Van Rijn, Arlind Kadra, Pieter Gijsbers, Neeratyoy Mallik, Sahithya Ravi, Andreas Müller, Joaquin Vanschoren, and Frank Hutter. Openml-python: an extensible python api for openml. *Journal of Machine Learning Research*, 22(100):1–5, 2021.

- [53] Janez Demšar. Statistical comparisons of classifiers over multiple data sets. *The Journal of Machine learning research*, 7:1–30, 2006.
- [54] William Jay Conover and Ronald L Iman. Multiple-comparisons procedures. informal report. Technical report, Los Alamos National Lab.(LANL), Los Alamos, NM (United States), 1979.
- [55] Milton Friedman. The use of ranks to avoid the assumption of normality implicit in the analysis of variance. *Journal of the american statistical association*, 32(200):675–701, 1937.
- [56] David R Cox. The regression analysis of binary sequences. *Journal of the Royal Statistical Society Series B: Statistical Methodology*, 20(2):215–232, 1958.
- [57] Corinna Cortes and Vladimir Vapnik. Support-vector networks. *Machine learning*, 20(3):273–297, 1995.
- [58] Jinsung Yoon, Yao Zhang, James Jordon, and Mihaela Van der Schaar. Vime: Extending the success of self-and semi-supervised learning to tabular domain. Advances in neural information processing systems, 33:11033–11043, 2020.
- [59] Yutaro Yamada, Ofir Lindenbaum, Sahand Negahban, and Yuval Kluger. Feature selection using stochastic gates. In *International conference on machine learning*, pages 10648–10659. PMLR, 2020.
- [60] Jintai Chen, Kuanlun Liao, Yao Wan, Danny Z Chen, and Jian Wu. Danets: Deep abstract networks for tabular data classification and regression. In *Proceedings of the AAAI Conference* on Artificial Intelligence, volume 36, pages 3930–3938, 2022.
- [61] Yury Gorishniy, Akim Kotelnikov, and Artem Babenko. Tabm: Advancing tabular deep learning with parameter-efficient ensembling. *arXiv preprint arXiv:2410.24210*, 2024.
- [62] Ruoxi Wang, Rakesh Shivanna, Derek Cheng, Sagar Jain, Dong Lin, Lichan Hong, and Ed Chi. Dcn v2: Improved deep & cross network and practical lessons for web-scale learning to rank systems. In *Proceedings of the web conference 2021*, pages 1785–1797, 2021.
- [63] Rohan Anil, Sandra Gadanho, Da Huang, Nijith Jacob, Zhuoshu Li, Dong Lin, Todd Phillips, Cristina Pop, Kevin Regan, Gil I Shamir, et al. On the factory floor: Ml engineering for industrial-scale ads recommendation models. arXiv preprint arXiv:2209.05310, 2022.
- [64] Günter Klambauer, Thomas Unterthiner, Andreas Mayr, and Sepp Hochreiter. Self-normalizing neural networks. *Advances in neural information processing systems*, 30, 2017.
- [65] Polina Kirichenko, Pavel Izmailov, and Andrew Gordon Wilson. Last layer re-training is sufficient for robustness to spurious correlations. In *The Eleventh International Conference on Learning Representations*, 2023.
- [66] Yury Gorishniy, Ivan Rubachev, and Artem Babenko. On embeddings for numerical features in tabular deep learning. Advances in Neural Information Processing Systems, 35:24991–25004, 2022.
- [67] Konstantin Schürholt, Boris Knyazev, Xavier Giró-i Nieto, and Damian Borth. Hyper-representations as generative models: Sampling unseen neural network weights. *Advances in Neural Information Processing Systems*, 35:27906–27920, 2022.
- [68] Konstantin Schürholt, Michael W Mahoney, and Damian Borth. Towards scalable and versatile weight space learning. In Forty-first International Conference on Machine Learning, 2024.
- [69] Laurens Van der Maaten and Geoffrey Hinton. Visualizing data using t-sne. *Journal of machine learning research*, 9(11), 2008.
- [70] Thomas G. Dietterich. Ensemble methods in machine learning. In *Multiple Classifier Systems*, pages 1–15, Berlin, Heidelberg, 2000. Springer Berlin Heidelberg.
- [71] Danny Wood, Tingting Mu, Andrew M Webb, Henry WJ Reeve, Mikel Lujan, and Gavin Brown. A unified theory of diversity in ensemble learning. *Journal of Machine Learning Research*, 24(359):1–49, 2023.

- [72] Joaquin Vanschoren, Jan N. van Rijn, Bernd Bischl, and Luis Torgo. Openml: Networked science in machine learning. *SIGKDD Explorations*, 15(2):49–60, 2013.
- [73] Christian Haslinger, Norbert Schweifer, Stephan Stilgenbauer, Hartmut Döhner, Peter Lichter, Norbert Kraut, Christian Stratowa, and Roger Abseher. Microarray gene expression profiling of b-cell chronic lymphocytic leukemia subgroups defined by genomic aberrations and vh mutation status. *Journal of Clinical Oncology*, 22(19):3937–3949, October 2004.
- [74] Arindam Bhattacharjee, William G Richards, Jane Staunton, Cheng Li, Stefano Monti, Priya Vasa, Christine Ladd, Javad Beheshti, Raphael Bueno, Michael Gillette, et al. Classification of human lung carcinomas by mrna expression profiling reveals distinct adenocarcinoma subclasses. *Proceedings of the National Academy of Sciences*, 98(24):13790–13795, 2001.
- [75] Dinesh Singh, Phillip G Febbo, Kenneth Ross, Donald G Jackson, Judith Manola, Christine Ladd, Pablo Tamayo, Andrew A Renshaw, Anthony V D'Amico, Jerome P Richie, et al. Gene expression correlates of clinical prostate cancer behavior. *Cancer cell*, 1(2):203–209, 2002.
- [76] Avrum Spira, Jennifer E Beane, Vishal Shah, Katrina Steiling, Gang Liu, Frank Schembri, Sean Gilman, Yves-Martine Dumas, Paul Calner, Paola Sebastiani, Sriram Sridhar, John Beamis, Carla Lamb, Timothy Anderson, Norman Gerry, Joseph Keane, Marc E Lenburg, and Jerome S Brody. Airway epithelial gene expression in the diagnostic evaluation of smokers with suspect lung cancer. *Nature Medicine*, 13(3):361–366, March 2007.
- [77] Gagan Bajwa, Ralph J DeBerardinis, Baomei Shao, Brian Hall, J David Farrar, and Michelle A Gill. Cutting edge: critical role of glycolysis in human plasmacytoid dendritic cell antiviral responses. *The Journal of Immunology*, 196(5):2004–2009, 2016.
- [78] Isabelle Guyon, Asa Gunn, Steve adn Ben-Hur, and Gideon Dror. Arcene. UCI Machine Learning Repository, 2004. DOI: https://doi.org/10.24432/C58P55.
- [79] Isabelle Guyon, Steve Gunn, Asa Ben-Hur, and Gideon Dror. Gisette. UCI Machine Learning Repository, 2004. DOI: https://doi.org/10.24432/C5HP5B.
- [80] V. I. Levenshtein. Binary Codes Capable of Correcting Deletions, Insertions and Reversals. *Soviet Physics Doklady*, 10:707, February 1966.

A Extended Notation

To ease navigation, Table 8 compiles the notation used in the paper. Lower-case bold letters (e.g. x) denote vectors, upper-case bold (e.g. X) denote matrices, and calligraphic letters (e.g. \mathcal{D}) denote sets unless noted otherwise (e.g., \mathcal{L} denotes a loss function). Readers may find it convenient to keep this table at hand while reading Section 3.

Table 8: Notation table.

Notation	Description
\mathcal{D}	A dataset.
$\mathcal{D}_{train},\mathcal{D}_{test},\mathcal{D}_{val}$	Training, test, and validation splits of \mathcal{D} .
$\mathcal{M}_{train},\mathcal{M}_{test},\mathcal{M}_{val}$	Meta-training, meta-test, and meta-validation collections of datasets.
N	Number of samples in a dataset.
d	Number of raw features in the data.
$oldsymbol{x}$	A single data point.
\boldsymbol{X}	Data matrix where each row is a data point.
K	Number of classes in the classification task.
\mathcal{Y}	$\{1,\ldots,K\}$
\boldsymbol{y}	Label vector for the data.
Y	Label matrix (one-hot encoded) for the data.
γ	Parameters of the GBDT and preprocessing pipeline.
$\Gamma_{\gamma}(\cdot)$	GBDT embedding function parameterized by γ .
T	Number of trees in the GBDT ensemble.
L_t	Number of leaves in tree t .
$l_i(m{x})$	Leaf index for data point x in a given tree.
M	Dimension of the GBDT embedding.
m	Dimension of the transformed feature space after initial transformations
	(either preprocessing-only, GBDT embedding, or their concatenation).
$oldsymbol{\psi}(oldsymbol{x})$	Output of the initial transformations.
$\sigma(\cdot)$	pointwise nonlinearity (e.g. ReLU).
r_{-}	Dimension after random feature expansion.
Ω	Random projection matrix used in the embedding stage.
d_{main}	Dimension of the fixed-size embedding used as input to the main network.
$oldsymbol{U}$	PCA transformation matrix reducing dimension from r to d_{main} .
ω	Parameters involved in the randomized fixed-size embedding projection.
$\Psi_{oldsymbol{\gamma},oldsymbol{\omega}}(\cdot)$	Complete embedding stage function that processes raw features into a fixed-size embedding.
\tilde{x}	Fixed-size embedding of a data point after the embedding stage.
θ	Parameters of the main network f_{θ} .
$f_{m{ heta}}$	Main network mapping embeddings \tilde{x} to output logits in \mathbb{R}^K .
$f_{m{ heta}}^{ ext{main}} \ f_{m{ heta}}^{ ext{out}}$	Layers of the main network (feature extractor) except the final classification layer.
$f_{m{ heta}}^{ ext{out}}$	Final classification layer of the main network.
ϕ	Parameters of the hypernetwork g_{ϕ} learned during meta-training.
$g_{m{\phi}}$	Hypernetwork that produces the main network parameters θ .
\mathcal{L}	Loss function.
α	Weight controlling the contribution of retrieval-augmented predictions.
τ	Temperature parameter for scaling similarities in the retrieval mechanism.
H	Penultimate layer representations from the main network.
S	Similarity matrix computed between query and context representations.
O	Output logits.

B Benchmarks

B.1 Dataset Characteristics

B.1.1 TabZilla Hard

Table 9 shows the number of samples and features included in the 36 datasets of the TabZilla Hard Benchmark Suite [12].

Table 9: Dimensions of the TabZilla Hard [12] datasets.

Dataset	# Samples	# Features
credit-g	1 000	21
jungle-chess	44 819	7
MiniBooNE	130 064	51
albert	425 240	79
electricity	45 312	9
elevators	16 599	19
guillermo	20 000	4 297
higgs	98 050	29
nomao	34 465	119
100-plants-texture	1 599	65
poker-hand	1 025 009	11
profb	672	10
socmob	1 156	6
audiology	226	70
splice	3 190	61
vehicle	846	19
Australian	690	15
Bioresponse	3 751	1 777
GesturePhase	9 872	33
SpeedDating	8 378	121
ada-agnostic	4 562	49
airlines	539 382	8
artificial-characters	10 218	8
colic	368	27
credit-approval	690	16
heart-h	294	14
jasmine	2 984	145
kc1	2 109	22
lymph	148	19
mfeat-fourier	2 000	77
phoneme	5 404	6
qsar-biodeg	1 055	42
balance-scale	625	5
cnae-9	1 080	857
mfeat-zernike	2 000	48
monks-problems-2	601	7

B.1.2 High-Dimensional Collection

While TabZilla Hard includes datasets with varying scales (148 to over 1 million samples) and moderate feature dimensionality (up to 4,297 features), we complement our evaluation with seven additional high-dimensional datasets going up to 19,993 features, primarily from biomedical applications, to demonstrate the scalability of iLTM to higher-dimensional problems, which are common in certain real-world domains. The seven datasets from our curated high-dimensional collection are

CLL_SUB_11 [73], Lung [74], Prostate-GE [75], SMK_CAN_187 [76], TOX-171 [77], Arcene [78] and Gisette [79] ¹, and their characteristics are listed in Table 10.

Table 10: High-dimensional datasets characteristics.

Dataset	# Samples	# Features	# Classes
CLL_SUB_111	111	11 340	3
Lung	203	3 312	5
Prostate_GE	102	5 966	2
SMK_CAN_187	187	19 993	2
TOX_171	171	5 748	4
Arcene	200	10 000	2
Gisette	7 000	5 000	2

B.1.3 Transfer Learning to Regression Datasets

For the regression benchmark, we use the publicly available datasets from [13], which have been also used in recent studies [20, 61], described in Table 11.

Table 11: Dimensions of the regression datasets.

Dataset	# Samples	# Features
nyc_taxi_green_dec_2016	581 835	9
elevators	16 599	16
fifa	18 063	5
wine_quality	6497	11
medical_charges	163 065	5
pol	15 000	26
MiamiHousing2016	13 932	14
year	515 345	90
cpu_act	8 192	21
isolet	7 797	613
Ailerons	13 750	33
Mercedes_Benz_Greener_Manufacturing	4 209	359
house_sales	21 613	15
particulate_matter_ukair_2017	394 299	6
analcatdata_supreme	4 0 5 2	7
OnlineNewsPopularity	39 644	59
superconduct	21 263	79
Brazilian_houses	10692	8

B.1.4 TabReD Benchmark

We further evaluate on the TabReD benchmark [22], which consists of eight datasets covering both classification and regression tasks. Table 12 summarizes their characteristics.

B.2 Extended Benchmark Results

B.2.1 TabZilla Hard Extended Results

Table 13 shows the detailed results for each of the top methods (according to Figure 3) across all datasets in the TabZilla Hard Benchmark [12]. Cells without numerical values available (NA) indicate datasets where the corresponding method failed to run due to out-of-memory errors (OOM), exceeding the time limit (TLE), or runtime or unknown errors (ERR). All errors for methods evaluated in [12] are marked with ERR, as the specific error type distinctions are not provided in the original source.

¹All of them are publicly available online at https://jundongl.github.io/scikit-feature/datasets

Table 12: Dimensions of the TabReD datasets. For the largest datasets, numbers in parentheses indicate the full dataset size, and we report the subset size used in TabReD to make hyperparameter tuning feasible, following the original benchmark [22].

Dataset	# Samples	# Features	Task Type
Sberbank Housing	28 000	392	Regression
Ecom Offers	160 000	119	Classification
Homesite Insurance	260 000	299	Classification
HomeCredit Default	381 000 (1.5M)	696	Classification
Cooking Time	319 000 (12.8M)	192	Regression
Delivery ETA	350 000 (17.0M)	223	Regression
Maps Routing	279 000 (13.6M)	986	Regression
Weather	423 000 (16.9M)	103	Regression

The bottom rows present the average test AUC across all 36 datasets, with missing cells (NA) handled using different computation methods that vary in how they favor methods with incomplete results. Notably, XGBoost [36] (top 4), TabPFNv2 [18] (top 2), and iLTM (top 1), executed successfully across all datasets without errors. Furthermore, iLTM achieved both the best average AUC rank, as demonstrated in Figure 3, but also the highest mean test AUC.

Table 13: AUC obtained by each of the top models (by average AUC mean rank as shown in Fig. 3) in all datasets of the TabZilla Hard Benchmark [12]. For the mean computation at the end, "NA=0" indicates that we computed the mean by imputing a 0 for the cells with an error, and "NA=row avg" means that we imputed the row average (i.e., average performance across methods for that dataset).

Dataset \ Method	r-MLP	RMLP	HF	RF	LGBM	TPFN1	r-RN	TabR	MNCA	CB	XGB	TabM	TPFN2	iLTM
Australian	0.924	0.890	0.900	0.938	0.941	0.932	0.926	0.932	0.910	0.942	0.935	0.931	0.940	0.943
Bioresponse	0.835	0.841	0.864	0.863	0.875	0.864	0.846	0.849	0.857	0.866	0.874	0.870	0.850	0.873
GesturePhase	0.728	0.892	0.829	0.854	0.902	0.829	0.787	0.941	0.918	0.862	0.899	0.916	0.927	0.907
MiniBooNE	0.980	0.987	0.964	0.976	0.986	0.968	0.975	0.988	MOO	0.984	0.985	0.989	0.980	0.988
SpeedDating	0.857	0.851	0.870	0.856	0.874	0.850	0.860	0.863	0.862	0.870	0.876	0.862	0.862	0.867
ada-agnostic	0.890	0.893	0.883	0.895	0.898	0.895	0.894	0.900	0.897	0.906	0.902	0.899	0.904	0.901
airlines	0.701	OOM	0.662	0.707	0.725	0.624	0.705	MOO	MOO	0.715	0.724	0.663	0.681	0.686
albert	0.746	OOM	0.689	0.726	ERR	0.689	0.760	MOO	MOO	0.777	0.759	OOM	0.726	0.748
artificial-characters	0.916	0.986	0.962	0.971	0.996	0.961	0.954	0.996	0.997	0.988	0.998	0.986	0.980	0.990
audiology	0.637	0.881	0.914	0.905	0.891	0.914	0.919	0.880	0.931	0.878	0.938	0.902	0.932	0.914
balance-scale	0.993	0.995	0.998	0.802	0.966	0.999	0.996	0.994	0.995	0.950	0.918	0.994	0.995	0.996
cnae-9	0.997	0.994	0.996	0.987	0.981	0.966	0.996	0.996	0.996	0.994	0.994	0.998	0.997	0.998
colic	0.877	0.824	0.856	0.903	0.895	0.878	0.871	0.870	0.869	0.905	0.912	0.847	0.916	0.893
credit-approval	0.922	0.889	0.910	0.934	0.927	0.935	0.931	0.930	0.924	0.939	0.945	0.932	0.939	0.939
credit-g	0.777	0.749	0.739	0.757	0.760	0.765	0.796	0.769	0.758	0.775	0.774	0.771	0.787	0.785
electricity	0.918	0.961	0.902	0.927	0.985	0.886	0.917	0.996	0.994	0.937	0.980	0.975	0.953	0.969
elevators	0.760	0.952	0.949	0.894	0.940	0.945	0.794	0.951	0.953	0.944	0.944	0.955	0.952	0.947
guillermo	0.781	0.897	0.724	0.878	ERR	0.828	0.794	MOO	MOO	ERR	0.907	0.913	0.845	0.897
heart-h	0.912	0.843	0.838	0.893	0.864	0.882	0.895	MOO	0.901	0.886	0.885	0.850	0.903	0.885
higgs	0.781	0.816	0.744	0.784	0.805	0.727	0.813	0.815	MOO	0.802	0.805	0.825	0.794	0.806
jasmine	0.851	0.854	0.858	0.870	0.864	0.869	0.854	0.875	0.864	0.869	0.869	0.873	0.887	0.873
jungle-chess	0.967	1.000	0.943	0.954	0.976	0.934	0.968	1.000	0.999	0.970	0.974	1.000	0.971	0.980
kc1	0.781	0.791	0.807	0.820	0.793	0.828	0.796	0.817	0.810	0.815	0.807	0.813	0.829	0.835
lymph	0.852	0.856	0.877	0.903	0.851	0.909	0.909	0.851	0.897	0.886	0.925	0.927	0.927	0.912
mfeat-fourier	0.973	0.984	0.982	0.980	0.981	0.988	0.978	0.980	0.983	0.983	0.983	0.987	0.991	0.985
mfeat-zernike	0.979	0.983	0.980	0.972	0.974	0.981	0.981	0.989	0.981	0.976	0.973	0.982	0.988	0.984
monks-problems-2	1.000	1.000	1.000	0.976	0.988	1.000	1.000	0.994	1.000	0.981	0.999	1.000	1.000	0.999
nomao	0.992	0.993	0.991	0.992	0.996	0.988	0.993	0.994	0.995	0.995	0.996	0.996	0.993	0.995
100-plants-texture	0.891	0.996	ERR	0.988	ERR	0.996	0.992	0.997	0.997	0.997	0.992	0.998	0.997	0.997
phoneme	0.948	0.956	0.942	0.955	0.959	0.942	0.936	0.964	0.968	0.945	0.960	0.962	0.968	0.966
poker-hand	0.546	OOM	0.589	ERR	ERR	0.527	ERR	MOO	MOO	0.934	0.860	0.995	0.671	0.803
profb	0.727	0.567	0.629	0.640	0.694	0.662	0.703	0.561	0.733	0.773	0.664	0.584	0.663	0.758
gsar-biodeg	0.923	0.922	0.936	0.926	0.918	0.941	0.927	0.921	0.898	0.930	0.928	0.936	0.939	0.937
socmob	0.984	0.968	0.975	0.977	0.977	0.978	0.985	0.989	0.967	0.986	0.988	0.989	0.990	0.985
splice	0.990	ERR	0.966	0.992	0.993	0.978	0.991	0.959	0.993	0.992	0.993	0.990	0.995	0.994
vehicle	0.830	0.946	0.967	0.927	0.920	0.969	0.952	0.967	0.966	0.934	0.934	0.956	0.973	0.960
Mean (NA=0)	0.866	0.804	0.851	0.870	0.808	0.884	0.872	0.792	0.773	0.886	0.911	0.891	0.907	0.914
Mean (NA=row avg)	0.866	0.892	0.878	0.891	0.900	0.884	0.893	0.901	0.906	0.909	0.911	0.911	0.907	0.914

We note that although here we provide the mean test AUC for completeness, average AUC can be biased by scale differences and missing data, while average ranking provides a more robust measure of relative performance across diverse datasets and supports rigorous statistical testing via the Nemenyi

test [53]. Critical difference diagrams with average rankings, as we have shown in Figure 3 are becoming the standard evaluation approach in tabular ML [12, 21, 61].

Table 14 presents the detailed AUC scores with standard deviations computed over the cross-validation folds for XGBoost [36], TabPFNv2 [18], and iLTM on the TabZilla Hard Benchmark [12]. While all three methods exhibit comparable standard deviations, iLTM shows slightly higher variability and TabPFNv2 demonstrates slightly lower variability across the cross-validation folds.

Table 14: Detailed AUC scores with standard deviations for XGBoost [36], TabPFNv2 [18], and iLTM on the TabZilla Hard Benchmark [12].

Dataset	XGBoost	TabPFNv2	iLTM
Australian	$0.9346_{\pm 0.0209}$	$0.9398_{\pm 0.0251}$	$0.9434_{\pm 0.0215}$
Bioresponse	$0.8741_{\pm 0.0160}$	$0.8496_{\pm 0.0247}$	$0.8729_{\pm 0.0174}$
GesturePhase	$0.8986_{\pm 0.0095}$	$0.9270_{\pm 0.0060}$	$0.9067_{\pm 0.0085}$
MiniBooNE	$0.9853_{\pm 0.0011}$	$0.9797_{\pm 0.0017}$	$0.9884_{\pm 0.0010}$
SpeedDating	$0.8764_{\pm 0.0114}$	$0.8617_{\pm 0.0119}$	$0.8665_{\pm 0.0126}$
ada-agnostic	$0.9019_{\pm 0.0187}$	$0.9043_{\pm 0.0144}$	$0.9010_{\pm 0.0174}$
airlines	$0.7242_{\pm 0.0024}$	$0.6812_{\pm 0.0026}$	$0.6902_{\pm 0.0029}$
albert	$0.7586_{\pm0.0027}$	$0.7256_{\pm 0.0018}$	$0.7592_{\pm 0.0024}$
artificial-characters	$0.9980_{\pm 0.0004}$	$0.9804_{\pm 0.0015}$	$0.9903_{\pm 0.0012}$
audiology	$0.9382_{\pm 0.0479}$	$0.9318_{\pm 0.0409}$	$0.9140_{\pm 0.0553}$
balance-scale	$0.9178_{\pm 0.0332}$	$0.9954_{\pm 0.0044}$	$0.9955_{\pm 0.0050}$
cnae-9	$0.9942_{\pm 0.0039}$	$0.9972_{\pm 0.0042}$	$0.9981_{\pm 0.0018}$
colic	$0.9116_{\pm 0.0480}$	$0.9163_{\pm 0.0470}$	$0.8926_{\pm 0.0603}$
credit-approval	$0.9446_{\pm 0.0391}$	$0.9394_{\pm 0.0371}$	$0.9387_{\pm 0.0434}$
credit-g	$0.7742_{\pm 0.0390}$	$0.7868_{\pm 0.0413}$	$0.7845_{\pm 0.0444}$
electricity	$0.9804_{\pm0.0013}$	$0.9533_{\pm 0.0025}$	$0.9692_{\pm 0.0019}$
elevators	$0.9437_{\pm 0.0052}$	$0.9524_{\pm 0.0051}$	$0.9469_{\pm 0.0054}$
guillermo	$0.9073_{\pm 0.0080}$	$0.8455_{\pm 0.0159}$	$0.8969_{\pm 0.0106}$
heart-h	$0.8849_{\pm 0.0439}$	$0.9025_{\pm 0.0374}$	$0.8853_{\pm 0.0438}$
higgs	$0.8051_{\pm 0.0072}$	$0.7938_{\pm 0.0074}$	$0.8063_{\pm0.0067}$
jasmine	$0.8694_{\pm 0.0181}$	$0.8873_{\pm 0.0122}$	$0.8734_{\pm0.0130}$
jungle-chess	$0.9742_{\pm 0.0015}$	$0.9707_{\pm 0.0059}$	$0.9799_{\pm 0.0013}$
kc1	$0.8073_{\pm 0.0480}$	$0.8293_{\pm 0.0290}$	$0.8347_{\pm 0.0364}$
lymph	$0.9252_{\pm 0.0415}$	$0.9267_{\pm 0.0645}$	$0.9120_{\pm 0.1028}$
mfeat-fourier	$0.9831_{\pm 0.0032}$	$0.9914_{\pm 0.0022}$	$0.9854_{\pm0.0028}$
mfeat-zernike	$0.9729_{\pm 0.0052}$	$0.9878_{\pm 0.0030}$	$0.9837_{\pm 0.0030}$
monks-problems-2	$0.9985_{\pm 0.0020}$	$1.0000_{\pm 0.0000}$	$0.9992_{\pm 0.0014}$
nomao	$0.9957_{\pm 0.0010}$	$0.9928_{\pm 0.0008}$	$0.9951_{\pm 0.0007}$
100-plants-texture	$0.9925_{\pm 0.0030}$	$0.9966_{\pm 0.0013}$	$0.9969_{\pm 0.0014}$
phoneme	$0.9602_{\pm 0.0093}$	$0.9678_{\pm 0.0081}$	$0.9662_{\pm 0.0106}$
poker-hand	$0.8602_{\pm 0.0385}$	$0.6707_{\pm 0.0141}$	$0.8025_{\pm 0.0207}$
profb	$0.6642_{\pm 0.0620}$	$0.6628_{\pm 0.0547}$	$0.7577_{\pm 0.0722}$
qsar-biodeg	$0.9283_{\pm 0.0312}$	$0.9393_{\pm 0.0298}$	$0.9366_{\pm 0.0301}$
socmob	$0.9879_{\pm 0.0095}$	$0.9900_{\pm 0.0079}$	$0.9854_{\pm 0.0063}$
splice	$0.9933_{\pm 0.0025}$	$0.9952_{\pm 0.0030}$	$0.9945_{\pm 0.0026}$
vehicle	$0.9344_{\pm 0.0102}$	$0.9734_{\pm 0.0073}$	$0.9603_{\pm 0.0104}$
Average	$0.9111_{\pm 0.0180}$	$0.9068_{\pm 0.0160}$	$0.9142_{\pm 0.0189}$

B.2.2 Extended Regression Results

Following the tuning and evaluation procedure used in [20, 61], each model is evaluated on each dataset under 15 random seeds. In Table 15 we report the mean test root mean square error (RMSE) and its standard deviation over the random seeds.

Table 15: Test RMSE (↓) scores across regression datasets.

Dataset	MLP	FT-Transformer	MLP-PLR	LightGBM	XGBoost	TabR	TabM	CatBoost	TabPFNv2	iLTM
Nyc-Taxi. 2016	0.3966 ± 0.001	0.3907 ± 0.001	0.3684 ± 0.002	0.3688 ± 0.000	0.3792 ± 0.000	0.3725 ± 0.009	0.3849 ± 0.001	0.3647 ± 0.001	0.4044 ± 0.006	0.3605 ± 0.000
Elevators	0.0051 ± 0.000	0.0050 ± 0.000	0.0024 ± 0.000	0.0020 ± 0.000	0.0020 ± 0.000	0.0019 ± 0.000	0.0019 ± 0.000	0.0020 ± 0.000	0.0019 ± 0.000	0.0018 ± 0.000
Fifa	$0.8025_{\pm0.001}$	0.7929 ± 0.002	$0.7945_{\pm 0.002}$	$0.7807_{\pm 0.001}$	0.7799 + 0.001	$0.7914_{\pm 0.003}$	$0.7953_{\pm 0.002}$	0.7835 + 0.001	$0.7821_{\pm 0.001}$	0.7796 ± 0.001
Wine Quality	$0.6716_{\pm 0.006}$	$0.6762_{\pm 0.004}$	$0.6543_{\pm 0.006}$	$0.6135_{\pm 0.002}$	$0.6039_{\pm 0.002}$	$0.6412_{\pm 0.008}$	$0.6328_{\pm 0.004}$	0.6088 ± 0.002	$0.6918_{\pm 0.002}$	$0.6055_{\pm 0.003}$
Medical Charges	$0.0816_{\pm 0.000}$	$0.0814_{\pm 0.000}$	$0.0811_{\pm 0.000}$	$0.0820_{\pm 0.000}$	$0.0825_{\pm 0.000}$	$0.0811_{\pm 0.000}$	$0.0812_{\pm 0.000}$	$0.0816_{\pm 0.000}$	$0.0813_{\pm 0.000}$	$0.0813_{\pm 0.000}$
Pol	5.6589 ± 0.206	2.7528 ± 0.133	2.6145 ± 0.127	4.2320 ± 0.036	4.2964 ± 0.022	2.5770 ± 0.159	3.0198 ± 0.061	3.6319 + 0.041	3.3983 + 0.107	2.8480 ± 0.032
Miamihousing2016	0.1614 ± 0.002	0.1517 ± 0.002	0.1502 ± 0.001	0.1461 ± 0.000	0.1440 ± 0.000	0.1392 ± 0.001	0.1477 ± 0.001	0.1417 ± 0.001	0.1348 ± 0.000	0.1386 ± 0.000
Year	$8.9635_{\pm 0.018}$	$9.0127_{\pm 0.020}$	$8.9274_{\pm0.013}$	$9.0200_{\pm 0.003}$	$9.0307_{\pm 0.003}$	$8.9721_{\pm0.011}$	8.8705 ± 0.004	9.0370 + 0.007	9.0328 + 0.022	$8.8884_{\pm0.010}$
Cpu Act	2.7119 ± 0.175	2.2356 + 0.081	$2.2700_{\pm 0.029}$	$2.2223_{\pm 0.015}$	$2.5237_{\pm 0.068}$	2.1278 + 0.052	$2.1402_{\pm 0.011}$	2.1239 + 0.015	$2.6881_{\pm 0.016}$	$2.1233_{+0.015}$
Isolet	$2.2226_{\pm 0.143}$	$2.3317_{\pm 0.163}$	$2.2240_{\pm 0.106}$	$2.7005_{\pm 0.013}$	$2.7567_{\pm 0.017}$	$1.9919_{\pm 0.134}$	$1.8433_{\pm 0.039}$	$2.8671_{\pm 0.014}$	$1.9657_{\pm 0.029}$	$1.9787_{\pm 0.032}$
Ailerons	0.0002 ± 0.000		0.0002 ± 0.000	0.0002 ± 0.000						
Mercedes Benz G. M.	8.3828 ± 0.060	8.2517 ± 0.068	8.3828 ± 0.060	8.2078 ± 0.043	8.2177 ± 0.019	8.3187 ± 0.075	8.2052 ± 0.026	8.1629 ± 0.022	8.1288 ± 0.008	8.2155 ± 0.026
House Sales	$0.1813_{\pm 0.001}$	$0.1687_{\pm 0.001}$	$0.1687_{\pm 0.001}$	$0.1692_{\pm 0.000}$	$0.1694_{\pm 0.000}$	0.1636 + 0.001	$0.1666_{\pm 0.000}$	0.1669 + 0.000	0.1599 + 0.000	0.1648 ± 0.000
Particulate-Mattr	$0.3766_{\pm 0.001}$	$0.3734_{\pm0.001}$	$0.3670_{\pm 0.001}$	$0.3637_{\pm 0.000}$	$0.3641_{\pm 0.000}$	0.3596 + 0.000	$0.3671_{\pm 0.001}$	$0.3647_{\pm 0.000}$	$0.3761_{\pm 0.001}$	$0.3641_{\pm 0.001}$
Analcatdata Supreme	0.0777 ± 0.002	0.0781 ± 0.001	0.0789 ± 0.003	$0.0778_{\pm 0.002}$	$0.0801_{\pm 0.003}$	$0.0807_{\pm 0.007}$	$0.0786_{\pm 0.002}$	$0.0780_{\pm 0.006}$	$0.0736_{\pm 0.001}$	$0.0817_{\pm 0.001}$
Onlinenewspopularity	$0.8620_{\pm 0.001}$	$0.8639_{\pm 0.002}$	$0.8618_{\pm 0.001}$	$0.8546_{\pm 0.000}$	$0.8545_{\pm 0.000}$	$0.8624_{\pm 0.001}$	$0.8579_{\pm 0.000}$	$0.8532_{\pm 0.000}$	$0.8532_{\pm 0.000}$	$0.8563_{\pm 0.000}$
Superconduct	10.7241 ± 0.062	10.7765 ± 0.111	10.5663 ± 0.058	10.1634 ± 0.012	10.1610 ± 0.020	10.3835 ± 0.056		10.2422 ± 0.022	9.9964 ± 0.025	
Brazilian Houses	$0.0487_{\pm 0.003}$		$0.0428_{\pm0.003}$	$0.0603_{\pm0.001}$	$0.0541_{\pm 0.001}$	$0.0451_{\pm0.005}$	$0.0418_{\pm0.001}$	$0.0468_{\pm 0.002}$	$0.0194_{\pm 0.001}$	$0.0534_{\pm0.001}$
Avg. Rank	5.8 ± 1.9	5.0 ± 2.0	4.6 ± 1.8	4.1 ± 1.8	4.0 ± 1.8	3.7 ± 1.9	3.4 ± 1.7	3.0 ± 1.4	2.9 ± 2.2	2.7 ± 1.6

B.3 Hyperparameter Search Spaces

iLTM The hyperparameter search space defined for iLTM is shown in Table 16. Note that fine-tuning and retrieval specific hyperparameters only have an effect if "Do finetuning" and "Do retrieval" are True, respectively. Similarly, GBDT embedding hyperparameters only have an effect if the preprocessing uses them, that is, if the preprocessing is not R.

Table 16: iLTM Hyperparameter Search Space

Hyperparameter	Type	Range	Default
General			
Preprocessing	Categorical	$\{R, X, C, RX, RC\}$	RX
Batch size	Categorical	{1024, 2048}	2048
Number of ensembles	Categorical	{1, 2, 4, 8, 12, 16, 20}	8
Feature bagging	Categorical	{True, False}	True
Finetuning			
Do finetuning	Categorical	{True, False}	True
Dropout	Categorical	$\{0.0, 0.15\}$	0.0
Max steps	Categorical	{4, 512, 1024}	1024
Learning rate	Log-uniform	$[10^{-6}, 10^{-2}]$	10^{-4}
Data	Categorical	{Bootstrap, Entire dataset}	Entire dataset
GBDT Embedding			
Data split	Categorical	{Dynamic, Entire dataset}	Dynamic
Fit for each predictor	Categorical	{True, False}	False
Number of estimators	Categorical	{100, 300}	100
Learning rate	Log-uniform	[0.01, 0.5]	GBDT model default
Retrieval			
Do retrieval	Categorical	{True, False}	True
Temperature τ	Uniform	[0.5, 3]	2.0
Weight α	Uniform	[0, 1]	0.5

LogReg-new Table 17 shows the hyperparameter search space defined for our re-execution of logistic regression.

Table 17: LogReg-new Hyperparameter Search Space

Hyperparameter	Type	Range	Default
Regularization (C)	Log-uniform	$[10^{-5}, 10^3]$ {L1, L2}	1.0
Penalty	Categorical		L2

HyperFast The hyperparameter search space for evaluating HyperFast [16] on the TabZilla Hard Benchmark [12] is presented in Table 18. These hyperparameter ranges were selected based on the recommendations provided in the official HyperFast repository documentation on GitHub².

Table 18: HyperFast Hyperparameter Search Space

Hyperparameter	Type	Range	Default
General Number of ensembles Batch size Neural network bias Stratified sampling	Categorical Categorical Categorical	{1, 4, 8, 16, 32} {1024, 2048} {True, False} {True, False}	Model default Model default Model default Model default
Optimization Optimization type Optimization steps Random seed	Categorical Categorical Categorical	{None, optimize, ensemble_optimize} {1, 4, 8, 16, 32, 64, 128} {0, 1, 2, 3, 4, 5, 6, 7, 8, 9}	Model default Model default Model default

TabR The hyperparameter search space for TabR [20] on the TabZilla Hard Benchmark [12] is presented in Table 19. These hyperparameter ranges were selected based on the recommendations provided in the paper.

Table 19: TabR Hyperparameter Search Space

Hyperparameter	Туре	Range
Model Parameters		
d_main	UniformInt	[96, 384]
context_dropout	Uniform	[0.0, 0.6]
dropout0	Uniform	[0.0, 0.6]
dropout1	Fixed	0.0
encoder_n_blocks	Categorical	$\{0, 1\}$
predictor_n_blocks	Categorical	{1, 2}
Optimizer		
optimizer type	Fixed	AdamW
learning rate	Log-uniform	$[3 \times 10^{-5}, 10^{-3}]$
weight decay	Categorical+Log-uniform	$\{0, [10^{-6}, 10^{-4}]\}$
Embeddings		
embedding type	Fixed	PLREmbeddings
n_frequencies	UniformInt	[16, 96]
d_embedding	UniformInt	[16, 64]
frequency_scale	Log-uniform	$[10^{-2}, 10^2]$
lite	Fixed	True

RealMLP The hyperparameter search space for RealMLP [10] on the TabZilla Hard Benchmark [12] is presented in Table 20. These hyperparameter ranges were selected based on the recommendations provided in the official RealMLP repository on GitHub³.

²https://github.com/AI-sandbox/HyperFast

³https://github.com/dholzmueller/pytabkit

Table 20: RealMLP Hyperparameter Search Space

Hyperparameter	Type	Range
Model Architecture		
num_emb_type	Categorical	{none, pbld, pl, plr}
add_front_scale	Categorical	{True (0.6), False (0.4)}
hidden_sizes	Categorical	{[256, 256, 256] (0.6), [64, 64, 64, 64, 64] (0.2), [512] (0.2)}
act	Categorical	{relu, selu, mish}
Training Parameter	s	
lr	Log-uniform	$[2 \times 10^{-2}, 3 \times 10^{-1}]$
p_drop	Categorical	$\{0.0 (0.3), 0.15 (0.5), 0.3 (0.2)\}$
wd	Categorical	$\{0.0, 2 \times 10^{-2}\}$
ls_eps	Categorical	$\{0.0(0.3), 0.1(0.7)\}$
PLR Embedding		
plr_sigma	Log-uniform	[0.05, 0.5]

TabM The hyperparameter search space for TabM [61] on the TabZilla Hard Benchmark [12] is presented in Table 21. These hyperparameter ranges were selected based on the recommendations provided in the paper.

Table 21: TabM Hyperparameter Search Space

Hyperparameter	Туре	Range
General Parameter	s (Both Cases)	
num_emb_type	Categorical	{none, pwl}
arch_type	Categorical	{tabm, tabm-mini}
k	Fixed	32
d_block	UniformInt	[64, 1024]
dropout	Categorical+Uniform	$\{0, [0.1, 0.5]\}$
weight_decay	Categorical+Log-uniform	$\{0, [10^{-4}, 10^{-1}]\}$
When num_emb_ty	pe = none	
n_blocks	UniformInt	[1, 6]
lr	Log-uniform	$[10^{-4}, 5 \times 10^{-3}]$
When num_emb_ty	pe = pwl	
n_blocks	UniformInt	[1, 5]
lr	Log-uniform	$[5 \times 10^{-5}, 3 \times 10^{-3}]$
num_emb_n_bins	UniformInt	[8, 32]

ModernNCA The hyperparameter search space for ModernNCA [21] on the TabZilla Hard Benchmark [12] is presented in Table 22. These hyperparameter ranges were selected based on the recommendations provided in the official ModernNCA repository on GitHub⁴.

TabPFNv2 The hyperparameter search space for TabPFNv2 [18] on the TabZilla Hard Benchmark [12] and the regression tasks is presented in Table 23. These hyperparameter ranges were selected based on the default output of tabpfn_extensions.hpo.TabPFNSearchSpace's get_classifier_space() and get_regressor_space(), as recommended by the official documentation.

⁴https://github.com/LAMDA-Tabular/TALENT

Table 22: ModernNCA Hyperparameter Search Space

Hyperparameter	Туре	Range
Model Architecture		
dim	UniformInt	[64, 1024]
dropout	Uniform	[0.0, 0.5]
d_block	UniformInt	[64, 1024]
n_blocks	Categorical	$\{0, 1, 2\}$
temperature	Fixed	1
sample_rate	Uniform	[0.05, 0.6]
Training Parameter	·s	
lr	Log-uniform	$[10^{-5}, 10^{-1}]$
weight_decay	Categorical+Log-uniform	$\{0, [10^{-6}, 10^{-3}]\}$
PLR Embeddings		
embedding_type	Fixed	PLREmbeddings
n_frequencies	UniformInt	[16, 96]
d_embedding	UniformInt	[16, 64]
frequency_scale	Log-uniform	[0.005, 10.0]
lite	Fixed	True

Table 23: TabPFNv2 Hyperparameter Search Space

Hyperparameter	Type	Range	Default
Number of estimators	UniformInt	L / - J	4
Softmax Temperature Average before Softmax	Categorical Categorical	{0.75, 0.8, 0.85, 0.9, 0.95, 1} {True, False}	0.9 False

C Discarding Criteria for Meta-Training Datasets

Meta-training a model on a large collection of diverse real tabular datasets requires careful dataset selection to avoid data leakage and ensure generalizability. In this section, we describe our rigorous criteria for discarding datasets (*i.e.*, excluding from our meta-training collection $\mathcal{M}_{\text{train}}$) to ensure *no overlap* and *minimizing any form of implicit leakage* with evaluation datasets. Below, we detail all the steps and checks involved in the discarding process.

C.1 Fundamental Constraints and Motivation

To maintain the integrity of our experimental setup, we enforce the following fundamental constraints:

- No dataset used for evaluation appears in the meta-training collection.
- Datasets that are highly similar to evaluation datasets, in name or structure, are discarded.
- Edge-case datasets that may introduce inconsistencies or unexpected biases are removed.
- Sample-level checks ensure no data leakage between meta-training and evaluation sets.

Given the complexity of tabular data hosting sites, where multiple versions and slight variations of the same dataset can exist, our discarding strategy extends beyond simple name filtering to include structural similarity and content-based exclusions. We address subtleties such as the presence of multiple copies of the same dataset (sometimes with slight differences in naming, features, or samples), and potential sample-level duplication.

C.2 High-Level Overview

We begin with a large unfiltered set \mathcal{P} of all open-source tabular classification datasets in OpenML [72, 52]. Then:

- 1. **Identification of evaluation datasets:** We define a set of *evaluation datasets* \mathcal{E} , as a reference panel for what must be excluded from the meta-training collection \mathcal{M}_{train} to avoid data leakage.
- 2. **Metadata Loading:** We read metadata about each candidate dataset (*e.g.* name, number of features, number of instances), together with its unique dataset identifier (*did*).
- 3. **Discard File Generation:** For each combination of "metadata" source and "evaluation datasets" we build a *discard file* that records whether a dataset is excluded and the reason for exclusion.
- 4. Name-Based Discards: We remove any dataset whose name (or partial/fuzzy variation) matches the name of an evaluation dataset. We also remove datasets whose name contains any evaluation dataset name as a substring, and any duplicates that differ only by version tags or small string variations.
- 5. **Size/Property-Based Discards:** Datasets with (i) too few or too many samples, (ii) too few or too many features, or (iii) identical shape to known evaluation datasets are discarded. We do not take into account the number of classes, meaning that we discard any potential dataset that has the same number of samples and features as any of the evaluation datasets. Although this may discard too many datasets that could actually be used for meta-training, we decided to keep this strong rule to avoid unexpected leakage.
- 6. **Sample-Level Checks:** Finally, we take a small sample (typically 5 random rows) from each evaluation dataset and compare it against each possible candidate dataset row to detect *sample-level* leakage.
- Final Inclusion Decision: The remaining datasets, after all discards, form our meta-training collection M_{train}.

C.3 Multi-Level Discarding Pipeline

The discarding pipeline consists of multiple stages, each imposing stricter criteria to filter out potential issues.

C.3.1 Evaluation Datasets Exclusion

We first ensure that any dataset *explicitly* used for evaluation is discarded. Let \mathcal{E} represent the set of evaluation datasets, as the union of the meta-validation datasets \mathcal{M}_{val} used for internal evaluation during meta-training, and the final meta-test collection \mathcal{M}_{test} used for final evaluation and benchmarking. These sets are disjoint:

$$\mathcal{E} = \mathcal{M}_{val} \cup \mathcal{M}_{test}, \quad \mathcal{M}_{val} \cap \mathcal{M}_{test} = \emptyset.$$

To obtain an intermediate filtered set of potential meta-training datasets, we discard all datasets that appear in \mathcal{E} from the initial unfiltered collection \mathcal{P} :

$$\mathcal{M}'_{\text{train}} = \mathcal{P} \setminus \bigcup_{\mathcal{D} \in \mathcal{E}} \mathcal{D}$$
 (6)

This first ensures that all explicitly known evaluation datasets are removed from meta-training.

C.3.2 Dataset Name Similarity Checks

Since OpenML contains multiple versions of the same dataset under slightly different names, we apply both exact and approximate matching techniques to identify and remove potential duplicates.

Exact Name Matching: We define a function $\sigma: \mathcal{S} \to \mathcal{S}$ that maps a dataset name to its sanitized version (*e.g.* lowercased and normalized), where \mathcal{S} is the set of all possible dataset names. Let $n_{\mathcal{D}}$ denote the name of a dataset \mathcal{D} , and $\mathcal{N}_{\mathcal{E}}^{\sigma}$ be the set of sanitized names corresponding to the evaluation datasets in \mathcal{E} :

$$\mathcal{N}_{\mathcal{E}}^{\sigma} = \{ \sigma(n_{\mathcal{D}}) \mid \mathcal{D} \in \mathcal{E} \}. \tag{7}$$

A dataset $\mathcal{D} \in \mathcal{M}'_{train}$ is discarded if its sanitized name belongs to $\mathcal{N}^{\sigma}_{\mathcal{E}}$:

$$\forall \mathcal{D} \in \mathcal{M}'_{\text{train}}, \quad \text{if } \sigma(n_{\mathcal{D}}) \in \mathcal{N}^{\sigma}_{\mathcal{E}}, \quad \text{then } \mathcal{M}'_{\text{train}} \leftarrow \mathcal{M}'_{\text{train}} \setminus \{\mathcal{D}\}. \tag{8}$$

Cleaning Common Keywords: To catch variations in dataset names, we define a preprocessing function $\tau:\mathcal{S}\to\mathcal{S}$ that removes common keywords such as small, medium, processed, classif, regression, version, etc., as well as years (e.g. 2016, 2017), digits, and other non-informative patterns. This is achieved using regular expressions (regex) to systematically strip out numbers and other non-alphabetical elements. Let $\mathcal{N}_{\mathcal{E}}^{\tau}$ be the set of sanitized names of evaluation datasets after applying this transformation:

$$\mathcal{N}_{\mathcal{E}}^{\tau} = \{ \tau(n_{\mathcal{D}}) \mid \mathcal{D} \in \mathcal{E} \}. \tag{9}$$

A dataset $\mathcal{D} \in \mathcal{M}'_{train}$ is discarded if its transformed name belongs to $\mathcal{N}^{\tau}_{\mathcal{E}}$:

$$\forall \mathcal{D} \in \mathcal{M}'_{\text{train}}, \quad \text{if } \tau(n_{\mathcal{D}}) \in \mathcal{N}_{\mathcal{E}}^{\tau}, \quad \text{then } \mathcal{M}'_{\text{train}} \leftarrow \mathcal{M}'_{\text{train}} \setminus \{\mathcal{D}\}. \tag{10}$$

Substring Matches: We remove any dataset $\mathcal{D} \in \mathcal{M}'_{\text{train}}$ whose name $n_{\mathcal{D}}$ contains the name of any evaluation dataset $\mathcal{D}' \in \mathcal{E}$ as a substring. Formally, let $n_{\mathcal{D}'}$ denote the name of an evaluation dataset $\mathcal{D}' \in \mathcal{E}$. A dataset $\mathcal{D} \in \mathcal{M}'_{\text{train}}$ is discarded if there exists $\mathcal{D}' \in \mathcal{E}$ such that $n_{\mathcal{D}'}$ is a substring of $n_{\mathcal{D}}$:

$$\forall \mathcal{D} \in \mathcal{M}'_{\text{train}}, \quad \text{if } \exists \mathcal{D}' \in \mathcal{E} \text{ such that } n_{\mathcal{D}'} \subseteq n_{\mathcal{D}}, \quad \text{then } \mathcal{M}'_{\text{train}} \leftarrow \mathcal{M}'_{\text{train}} \setminus \{\mathcal{D}\}. \tag{11}$$

Approximate String Matching Using Similarity Measures: To account for minor variations in dataset names, we employ two similarity measures to identify and discard datasets with names that are approximately similar to those in \mathcal{E} :

• Levenshtein Similarity: Let $L_{\text{sim}}: \mathcal{S} \times \mathcal{S} \to [0,1]$ denote the normalized Levenshtein similarity, defined as:

$$L_{\text{sim}}(n_1, n_2) = 1 - \frac{L(n_1, n_2)}{\max(|n_1|, |n_2|)},$$
(12)

where $L(n_1, n_2)$ is the Levenshtein distance [80] between strings n_1 and n_2 , which measures the minimum number of edits (insertions, deletions, or substitutions) required to transform one string into the other, and $|n_1|, |n_2|$ are their respective lengths. A dataset $\mathcal{D} \in \mathcal{M}'_{\text{train}}$ is discarded if its name $n_{\mathcal{D}}$ satisfies:

$$L_{\text{sim}}(n_{\mathcal{D}}, n_{\mathcal{D}'}) \ge \lambda, \quad \exists \mathcal{D}' \in \mathcal{E},$$
 (13)

where $\lambda \in [0, 1]$ is a similarity threshold.

• Token Sort Ratio (TSR)⁵: Let TSR : $\mathcal{S} \times \mathcal{S} \to [0,1]$ denote the token sort ratio, a fuzzy matching technique that tokenizes, reorders, and compares the words in two names in a slightly different manner than L_{sim} . A dataset $\mathcal{D} \in \mathcal{M}'_{\text{train}}$ is discarded if its name $n_{\mathcal{D}}$ satisfies:

$$TSR(n_{\mathcal{D}}, n_{\mathcal{D}'}) > \lambda, \quad \exists \mathcal{D}' \in \mathcal{E}.$$
 (14)

We use a similarity threshold of $\lambda=0.8$ for both measures. Datasets whose names exceed this threshold for any of the two similarity metrics, for any evaluation dataset $\mathcal{D}' \in \mathcal{E}$ are discarded, as they indicate high redundancy with evaluation datasets. This approach ensures that even slightly renamed or partially obfuscated duplicates are recognized.

C.3.3 Structural Filtering

Datasets are further discarded if their structural properties are too similar to evaluation datasets. Let $N_{\mathcal{D}}$ and $F_{\mathcal{D}}$ denote the number of instances and features, respectively, of a dataset \mathcal{D} . Given an evaluation dataset $\mathcal{D}' \in \mathcal{E}$ with $N_{\mathcal{D}'}$ instances and $F_{\mathcal{D}'}$ features, a candidate training dataset $\mathcal{D} \in \mathcal{M}'_{\text{train}}$ is discarded if it shares the same number of samples and features as \mathcal{D}' :

$$(N_{\mathcal{D}} = N_{\mathcal{D}'}) \wedge (F_{\mathcal{D}} = F_{\mathcal{D}'}), \quad \exists \mathcal{D}' \in \mathcal{E}.$$
(15)

This prevents subtle leakage from datasets that might be completely relabeled but structurally identical. Although this approach can be overly conservative in certain edge cases (*e.g.* distinct datasets that happen to have identical shapes), we enforce it to avoid potential near-duplicates or disguised versions of the same data.

C.3.4 Edge Case Removal

Independently of potential overlap with evaluation datasets, we remove certain outliers from meta-training based on their structural properties. A dataset $\mathcal{D} \in \mathcal{M}'_{train}$ is discarded if it satisfies any of the following conditions:

- Fewer than 2 features: $F_{\mathcal{D}} < 2$.
- Fewer than 10 samples: $N_{\mathcal{D}} < 10$.
- More than 100,000 features: $F_D > 100,000$.
- More than 1,000,000 samples: $N_D > 1,000,000$.

C.3.5 Sample-Level Leakage Detection

One of the more stringent steps in our pipeline is a final row-by-row comparison of actual data samples between meta-training and evaluation datasets. This ensures that no training data is implicitly represented in evaluation benchmarks.

Let $\mathcal{D}' \in \mathcal{E}$ denote an evaluation dataset with feature matrix $\mathbf{X}_{\mathcal{D}'}$, where each row $\mathbf{x}_{\mathcal{D}'} \in \mathbf{X}_{\mathcal{D}'}$ represents a sample. For each \mathcal{D}' , we sample k=5 rows uniformly at random to form a subset $S_{\mathcal{D}'} = \{\mathbf{x}_{\mathcal{D}'}^{(1)}, \dots, \mathbf{x}_{\mathcal{D}'}^{(k)}\}$. Let $\mathbf{X}_{\mathcal{D}}$ be the feature matrix of a candidate training dataset $\mathcal{D} \in \mathcal{M}'_{\text{train}}$,

⁵https://github.com/seatgeek/thefuzz

combining all its splits (train, validation, test). We discard \mathcal{D} if **any** of the sampled evaluation rows matches one of its rows:

$$\exists \mathcal{D}' \in \mathcal{E}, \quad \exists x_{\mathcal{D}'} \in S_{\mathcal{D}'}, \quad \exists x_{\mathcal{D}} \in X_{\mathcal{D}} \quad \text{such that} \quad x_{\mathcal{D}'} \equiv x_{\mathcal{D}} \land F_{\mathcal{D}} = F_{\mathcal{D}'},$$
 (16)

where $x_{\mathcal{D}'} \equiv x_{\mathcal{D}}$ denotes that the multiset of feature values in $x_{\mathcal{D}'}$ is identical to that of $x_{\mathcal{D}}$, regardless of column order. We use a multiset (counter-based) comparison of feature values to detect matches irrespective of the original column ordering. Note that the candidate dataset \mathcal{D} is discarded immediately upon detection of any matching row to save computation time.

Although this check can be computationally expensive to run, it provides an extra safeguard against including any datasets that merely differ in feature-column arrangement but contain identical samples.

C.4 Conclusion

The final meta-training set $\mathcal{M}_{\text{train}}$ consists of datasets in $\mathcal{M}'_{\text{train}}$ that pass all discarding conditions. Defining each discard criterion as $\mathrm{DC}_i(\mathcal{D})$, where $\mathrm{DC}_i(\mathcal{D})$ means dataset \mathcal{D} meets the i-th condition, we have:

$$\mathcal{M}_{\text{train}} = \left\{ \mathcal{D} \in \mathcal{M}'_{\text{train}} \mid \neg \left(DC_1(\mathcal{D}) \vee DC_2(\mathcal{D}) \vee \dots \right) \right\}. \tag{17}$$

This ensures that only datasets not meeting any of the discard criteria are included in the final meta-training set. By following this detailed pipeline, we achieve a robust filtering of meta-training data, completely avoiding duplicates or near-duplicates of evaluation datasets. The procedure we describe is conservative but necessary to prevent inadvertent data leakage in large-scale tabular meta-learning experiments.